International Journal of Pharmaceutics: X 4 (2022) 100130

Contents lists available at ScienceDirect

International Journal of Pharmaceutics: X

journal homepage: www.sciencedirect.com/journal/international-journal-of-pharmaceutics-x

Protein sustained release from isobutyramide-grafted stellate mesoporous silica nanoparticles

Joëlle Bizeau [a], Alexandre Adam [a], Clémence Nadal [a], Grégory Francius [b], David Siniscalco [b], Matthias Pauly [c], Sylvie Bégin-Colin [a], Damien Mertz [a,*]

[a] Institut de Physique et Chimie des Matériaux de Strasbourg (IPCMS), UMR-7504 CNRS-Université de Strasbourg, 23 rue du Læss, BP 34 67034, Strasbourg, France
[b] Laboratoire de Chimie Physique et Microbiologie pour les Matériaux et l'Environnement (LCPME), UMR 7564 CNRS-Université de Lorraine, 405 rue de Vandoeuvre, 54600 Villers-lès-Nancy, France
[c] Université de Strasbourg, CNRS, Institut Charles Sadron (UPR22), 23 rue du Loess, 67034, Strasbourg BP 84047, France

ARTICLE INFO

Keywords:
Protein sustained release
Protein quantification
Stellate mesoporous silica
Protein-surface interactions
Nanoparticles

ABSTRACT

Proteins are great therapeutic candidates as endogenous biomolecules providing a wide range of applications. However, their delivery suffers from some limitations and specifically designed delivery systems having an efficient protein anchoring and delivery strategy are still needed. In this work, we propose to combine large pore stellate mesoporous silica (STMS) with isobutyramide (IBAM), as a "glue" molecule which has been shown promising for immobilization of various biomacromolecules at silica surface. We address here for the first time the ability of such IBAM-modified NPs to sustainably deliver proteins over a prolonged time. In this work, a quantitative loading study of proteins (serum albumin (HSA), peroxidase (HRP), immunoglobulin (IgG) and polylysine (PLL)) on STMS@IBAM is first presented using three complementary detection techniques to ensure precision and avoid protein quantification issues. The results demonstrated a high loading capacity for HSA and HRP ($\geq$ *ca.* 350 $\mu g.mg^{-1}$) but a moderate one for IgG and PLL. After evaluating the physicochemical properties of the loaded particles and their stability over scaling-up and washings, the ability of STMS@IBAM to release proteins over prolonged time was evaluated in equilibrium (static) and flow mimicking (dynamic) conditions and at different temperatures (25, 37, 45 °C). Results show not only the potential of such "glue" functionalized STMS to release proteins in a sustained way, but also the retention of the biological activity of immobilized and released HRP, used as an enzyme model. Finally, an AFM-force spectroscopy study was conducted to decipher the interactions between IBAM and proteins, showing the involvement of different interactions in the adsorption and release processes.

1. Introduction

Proteins have been studied for decades as therapeutic agents due to several advantages over synthesized molecules or polymers. Indeed, there are endogenous biomacromolecules, meaning that there are biocompatible and biodegradable and that their degradation products are known as non-toxic. In addition, they are involved in a very broad range of biological processes, with specified functions such as activation and inhibition of cellular pathways or biocatalysis, giving also a large choice for therapeutic applications (cancer therapy, diabetes treatment, tissue engineering, etc). However, among their disadvantages, proteins suffer from a short half-life and a conformational fragility, making them delicate for a direct use in therapy. Thus, there is a need to develop protein delivery systems (PDS) able to load and deliver them at the injured site (Bizeau and Mertz, 2021; Leader et al., 2008; Putney and Burke, 1998; Yu et al., 2016).

The loading of proteins in PDS can be performed using three main ways: i) by blending prior to formation of the PDS, ii) by immersion after formation, which can also be done by dipping or layer-by-layer coating of proteins on the system, and iii) by immobilization using a covalent bond. The release of the proteins is also a key aspect of such systems. It can be performed by a natural diffusion of the protein out of the PDS, or the PDS can be designed in order to be sensitive to a local stimulus such as pH (Vander Straeten and Dupont-Gillain, 2020; Wu et al., 2017a; Zhang et al., 2017), redox (Hsiao et al., 2017; McAvan et al., 2017), reactive oxygen species (Tong et al., 2018), glucose (Chen et al., 2017)

* Corresponding author.
E-mail address: damien.mertz@ipcms.unistra.fr (D. Mertz).

https://doi.org/10.1016/j.ijpx.2022.100130
Received 2 September 2022; Accepted 5 September 2022
Available online 9 September 2022

or protease degradation (Mumcuoglu et al., 2018). The use of external stimuli, such as light (Wang et al., 2017), near-infrared irradiation (Tuncaboylu et al., 2018), magnetic field (Omar et al., 2017) or mechanical stress (Xu et al., 2017; Zhang et al., 2019) is of great interest to better control the release of proteins at a given site. Thus, since decades, PDS are developed in a range of different formulations to answer the challenges of the field: nano and microparticles (NPs/MPs), hydrogels, fibers, films, microneedle patches and macroporous scaffolds. In a very general way, hydrogels, films and microneedle patches are developed for the regeneration of soft tissues, such as skin or myocardiac tissues, while fibers are used to regenerate oriented tissues, notably nerves and cartilage, but also the skin. Regarding microporous scaffolds, they are widely developed for hard tissue regeneration, meaning mainly bones (Bizeau and Mertz, 2021). Combination of these systems are also formulated and studied, notably with NPs or MPs as it helps to control more finely the release of proteins. Moreover, these latter are of particular interest when cellular uptake or the crossing of the blood-brain barrier are required (Kobsa and Saltzman, 2008), making them a PDS of choice for applications such as cancer or diabetes treatment (Bizeau and Mertz, 2021).

Among PDS, mesoporous silica NPs (MSNs) are promising. Mesoporous silica materials (MCM, *Mobil* composition of matter) have first been synthesized in the 1990's by Mobil Corporation laboratories and first proposed as a drug delivery system in 2001 by Vallet-Regí *et al* (Manzano and Vallet-Regí, 2020). In this same year 2001, the synthesis of MSNs was reported for the first time by different groups. (Wu et al., 2013) Since then, MSNs are widely studied for drug delivery due to several structural and physicochemical advantages. Indeed, NPs size and porous matrix features (pore size, volume and morphology) can be easily tuned. These particles also have a high surface area and it is easy to functionalize them by reaction of silanes having versatile chemical end-groups with the silanol groups largely present on their surface. In addition, the US Food and Drug Administration (FDA) accepted silica as "Generally Recognized As Safe", making it a great candidate for medical application (Argyo et al., 2014; Manzano and Vallet-Regí, 2020; Tang et al., 2012). Among silica NPs and MPs, stellate mesoporous silica NPs (STMS NPs) are particularly attractive as protein carriers, as they present a large specific surface area (500 $m^2.g^{-1}$) and pore size of *ca.* 15 nm especially adapted for protein dimensions (Zhang et al., 2013a). These STMS were shown to be easily modifiable and thus were used as bimodal imaging probes by functionalizing them with quantum dots (Perton et al., 2019b) or for iron removal from brain mimicking fluid by binding a deferrioxamine ligand on their surface (Duenas-Ramirez et al., 2020). In these last cases, the binding was of covalent nature, but for ensuring therapeutics loading and release, the interactions between silica NPs and the drug has to be better finely tailored. Indeed, ideal drug release systems should interact with the therapeutics in a way that is strong enough to ensure efficient loading but also labile enough to allow their controlled release. The surface functionalization of silica NPs thus appears to be a key step in drug delivery approach and the design of a smart anchoring strategy acting as glue molecules allowing the efficient retention and then prolonged release of proteins still remains a challenge.

In this work, we propose to test an original intermolecular glue strategy at NP interface, based on isobutyramide (IBAM) binders, to evaluate its potential for protein sustained release in biological aqueous buffer. IBAM groups were previously shown to form a tight non-covalent layer with a range of proteins but also other biopolymers such as nucleic acids or polysaccharides (Mertz et al., 2011, 2012b). This strategy was demonstrated with several silica shapes and porosities. Furthermore, upon silica removal, the IBAM groups were able to bind and physically crosslink the biomacromolecules, leading to the formation of a variety of self-standed biopolymers/protein hollow capsules biologically active or loaded with therapeutic molecules (Mertz et al., 2014; Mertz et al., 2012a; Mertz et al., 2011). Although some protein coatings on IBAM-functionalized non porous silica were studied to demonstrate the formation of such non-covalently biopolymer self-supported capsules, neither the full quantification of protein loading within IBAM-functionalized large pore mesoporous silica NPs nor the ability of these NPs to release the loaded proteins over prolonged time were yet studied.

Herein, these questions were investigated in depth by using four proteins: human serum albumin (HSA), horseradish peroxidase (HRP), immunoglobulin G (IgG) and poly-L-lysine (PLL). HSA was chosen as a transport protein widely present in the body (He and Carter, 1992; Sudlow et al., 1975; Wiberg et al., 2004). In addition, it is also widely used as a model protein in the literature. HRP was chosen in order to have a protein with a biological activity. Indeed, this enzyme extracted from horseradish roots is able to catalyze the oxidation of a variety of substrate in presence of hydrogen peroxide (H_2O_2). It is notably the most studied enzyme of the plant peroxidase superfamily (Huang et al., 2018; Schejter et al., 1976). The IgG was also selected as it is widely present in the body. It is actually the most present protein with HSA and the most represented of the five immunoglobulin classes (80%) and plays an important role in the immune system as it is an antibody (Papadea and Check, 1989; Wiberg et al., 2004). The last chosen protein is PLL, a polypeptide that was shown to enhance cell adhesion, which also makes it a good candidate for therapeutic applications such as tissue regeneration (Zhang et al., 2013b; Zheng et al., 2019). These four proteins were chosen not only for their properties but also because they offer a large range of molecular weight and isoelectric point values.

A first aim of this work was to quantify the loading capacity of these proteins or polypeptides on STMS@IBAM. It is worth noting that the quantification of proteins is known to be delicate due to several parameters such as the concentration (detection limit) and structure (amino-acid sequence) of the protein in the sample and the composition of the sample (presence of other molecules such as salt, buffer, detergent, solvent, chelating/reducing/thiol-containing agent). Hence here, three different detections techniques were used to determine with accuracy and precision the loading capacity in our NPs as a function of their feed weight ratio (FWR) *i.e.* the quantity of proteins given to the silica carrier. These three techniques consisted in i) labelling the proteins with fluorescein isothiocyanate (FITC), ii) using their intrinsic fluorescence due to the tryptophan residue in their amino acid sequence and iii) using the reactivity of peptide bonds in the Bicinchoninic acid (BCA) assay. Secondly, after a preliminary study which allowed to set the physicochemical properties and the chemical engineering conditions of the protein-coated NPs (such as protein payload, colloidal stability, surface charge, scaling-up and the stability over consecutive washings), the ability of the NPs for sustained protein release from STMS@IBAM NPs in HEPES buffer (pH 7.4, 50 $mmol.L^{-1}$) was evaluated. HSA and HRP protein release were investigated in depth over one week at equilibrium (under static conditions) and by changing buffer each 24 h (dynamic conditions) and at several temperatures (25, 37, 45 °C). With the aim to validate the bioactivity of the proteins, the enzymatic activity of HRP adsorbed on the NPs or released in the aqueous solution was assessed. Finally, the nature of interactions between IBAM groups and the proteins was explored at the protein scale. In order to provide insights into the possible interactions involved in the adsorption of proteins with IBAM groups, atomic force microscopy (AFM) in force spectroscopy mode was conducted with HSA- and HRP-functionalized tips to obtain force map on IBAM-functionalized silica surface as compared to bare silica and discuss the potential interactions involved in the protein binding and release.

The main steps of this work are presented in Scheme 1.

2. Materials and methods

2.1. Materials

All products were used as provided. Citric acid ($C_6H_8O_7$, CAS 77–92-9), ethanolamine hydrochloride ($C_2H_7NO{\cdot}Cl$, CAS 2002-24-6), HEPES

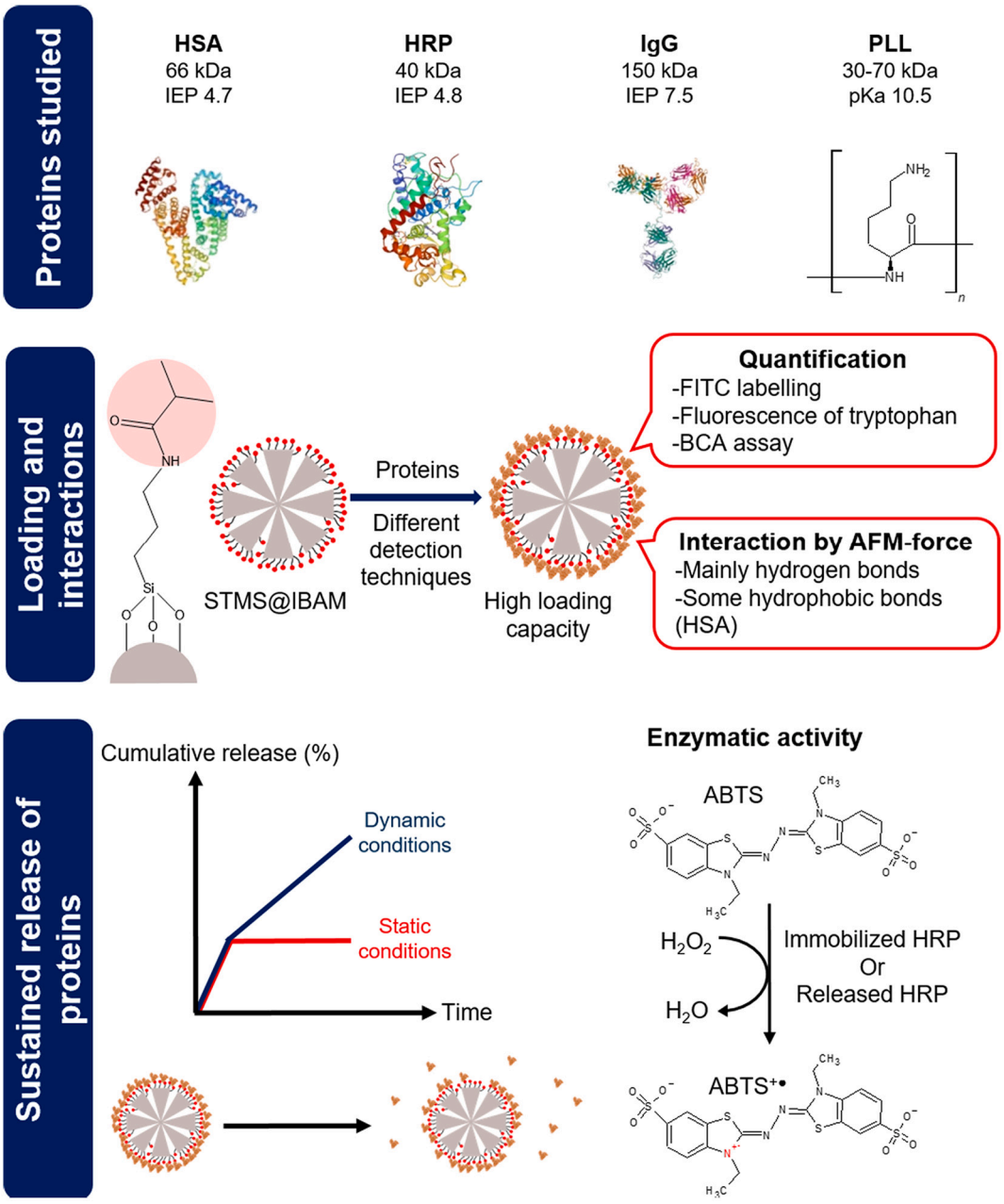

Scheme 1. Representative scheme of the study and its main results. Representation of HSA, HRP and IgG provided on Protein Data Base by Sugio et al. (Sugio et al., 1999), Berglund et al. (Berglund et al., 2002) and Saphire et al. (Saphire et al., 2001) respectively.

(CAS 7365-45-9), triethylamine (Et_3N, CAS 121–44-8) and sodium carbonate ($NaHCO_3$, CAS 144–55-8) were purchased from Sigma Aldrich. Cetyltrimethylammonium p-toluene sulfonate (CTATos, CAS 138–32-9), human serum albumin (HSA, 66,478 $g.mol^{-1}$, CAS 70024–90-7), FITC-labelled Immunoglobulin G from human serum (IgG^{FITC}, CAS ND) and Trizma® base (AHMPD, CAS 77–86-1) were purchased from Sigma life science. Anhydrous absolute ethanol (EtOH, CAS 64–17-5), chloroform ($CHCl_3$, CAS 67–66-3), dimethylformamide (DMF, CAS 68–12-2) and sulfuric acid 96% (H_2SO_4, CAS 7664-93-9) were purchased from Carlo Erba Reagents. Peroxidase from horseradish (HRP, 40,000 $g.mol^{-1}$, ~150 $U.mg^{-1}$, CAS 9003-99-0), IgG from human serum (Mw 150,000 $g.mol^{-1}$ (Papadea and Check, 1989), CAS ND) and poly-L-lysine hydrobromide (30,000–70,000 $g.mol^{-1}$, CAS 25988–63-0) were purchased from Sigma. (3-aminopropyl)triethoxysilane (APTES, CAS 919–30-2) and isobutyrylchloride (IBC, CAS 79–30-1) were purchased from Aldrich. Sodium cyanoborohydride ($NaCNBH_3$, CAS 25895–60-7) and tetraethylorthosilicate (TEOS, CAS 78–10-4) were purchased from Aldrich chemistry. Acetal-PEG-NHS was purchased from Linz University (Austria), ammonium hydroxide solution (25% in water), (NH_4OH, CAS 1336-21-6) from Fluka, 2,2′-azino-bis(3-ethylbenzothiazoline-6-sulfonic acid) diammonium salt (ABTS, CAS 30931–67-0) from Alfa Aesar, dimethyl sulfoxide (DMSO, CAS 67–68-5) from Roth, fluorescein isothiocyanate (FITC, CAS 3326-32-7) from TCI, hydrogen peroxide 35% (H_2O_2, CAS 7722-84-1) from Acros organics and the Micro™ protein assay kit from Thermoscientific.

It has to be noted that some products were also purchased from other providers for AFM: H_2O_2 30% and DMSO were purchased from VWR chemical, HEPES was purchased from Sigma life science, sulfuric acid 95–98% from Sigma Aldrich, and Et_3N from Fluka analytical.

2.2. Synthesis of STMS

The protocol was used as described previously (Bizeau et al., 2021; Duenas-Ramirez et al., 2020; Perton et al., 2019a). CTATos (3.8 g) and AHMPD (0.436 g) were introduced in a 500 mL flask with 200 mL of deionized water (dH_2O) and stirred at 75 °C up to full dissolution (about 30 min). Then, TEOS (30.2 g) was added in the flask and the mixture was left for reaction under stirring for 2 h at 75 °C. A white precipitate could then be observed. The mixture was cooled to room temperature then filtered under vacuum. The CTATos was then removed by calcination at 550 °C for 10 h, giving around 7 g of white powder. A mortar was then used to crush a part of the STMS NPs in a fine powder prior to suspend it in around 20 mL of EtOH in a 50 mL tube. Sonication and vortex were used to suspend the maximum of NPs. A fast centrifugation cycle (30 s, the time for the centrifuge to accelerate) was then used to make the residual aggregates fall and the supernatant containing well suspended NPs was transferred to a new tube. A known volume of the solution was dried to calculate the STMS concentration and the tube was then stored on a wheel until use.

2.3. Functionalization of STMS with APTES: STMS@APTES

Basically, 20 mg of STMS was dispersed in 5.5 mL of EtOH in a 15 mL tube. Then, NH_4OH 25% (0.3 mL) and APTES (1.25 mL) were added sequentially to the tube. The solution was homogenized with a vortex and then placed on the wheel for 2 h of stirring. Then the NPs were centrifuged (11,000 *g*, 10 min) and washed (2*7 mL EtOH and 2*7 mL DMF).

2.4. Functionalization of STMS@APTES with IBAM: STMS@IBAM

The previously prepared 20 mg of STMS@APTES was dispersed in 3 mL of DMF in a 15 mL tube while a solution of IBC (0.55 mL) and DMF (3 mL) was prepared in a 5 mL tube. Then, Et_3N (0.4 mL) and the IBC solution were added sequentially to the tube containing the particles. The solution turned orange and was homogenized and degassed using sonication and vortex. The tube was placed on the wheel for 2 h for reaction and then around 3 mL of dH_2O was added to the solution to dissolve the organic salt. The NPs were then centrifuged (11,000 *g*, 10 min) and washed (2*7 mL of DMF and 2*7 mL of EtOH). The NPs were stored in EtOH on the wheel for a maximum of three days.

2.5. FITC labelling of proteins: $protein^{FITC}$

Proteins were labelled with FITC using a molar ratio of 2 FITC for 1 protein and the solutions were protected from light during all the procedure. Basically, 50 mg of protein was dissolved in 5 mL of $NaHCO_3$ buffer (0.1 $mol.L^{-1}$, pH 8.5) to obtain a 10 $mg.mL^{-1}$ solution. Then, the adequate volume of a 10 $mg.mL^{-1}$ solution of FITC in DMSO was added and the solution was stirred for 1 h. The solution was then dialyzed for 2 days in dH_2O to remove the free FITC with a change of water every 2 h. Finally, the solution was collected and the final volume measured to calculate the exact concentration taking into consideration the swelling of the dialysis bag. The solution was then stored at −20 °C.

2.6. Loading of STMS@IBAM with protein: STMS@IBAM@Protein

The procedure was the same for unlabelled and labelled proteins, with a protection from light with aluminium foil in the case of labelled protein. In a typical protocol, the previously prepared 20 mg of STMS@IBAM was washed twice with 7 mL of dH_2O (centrifugation 11,000 *g*, 10 min) prior to be resuspended in 10 mL of dH_2O. A volume of 1 mL was then transferred in 1.5 mL tube (2 mg of particles). The NPs were then centrifuged (11,000 *g*, 10 min) and resuspended in 50 μL of dH_2O. Then 500 μL of protein solutions at known concentrations were added to the tube. The solutions were vortexed and then stirred for 1 h. The NPs were then centrifuged (11,000 *g*, 10 min) and the loading supernatant collected for quantification.

2.7. Scale-up and standardized washings

A scale-up had to be done for the rest of the study. Thus, 35 mg of STMS was first functionalized with APTES (9.625 mL of EtOH, 0.525 mL of NH_4OH, 2.1876 mL of APTES) and then with IBAM (5.25 mL of DMF for resuspension, 0.9625 mL of IBC mixed with 5.25 mL of DMF, 0.7 mL of Et_3N, around 5 mL of dH_2O). In both case, the procedure was conducted in a 50 mL tube and the volume of solvent used for the washing was increased to 10 mL.

For the loading of protein, a fixed FWR of 50% for HSA, 60% for IgG and HRP and 100% for PLL was chosen. The 35 mg of STMS@IBAM was centrifuged (11,000 *g*, 10 min) and resuspended in 7 mL of dH_2O in order to have a concentration of 5 $mg.mL^{-1}$. A volume of 2 mL was then transferred in 5 mL tubes (10 mg) and the NPs were washed twice with 1 mL of dH_2O prior to be resuspended in 250 μL of dH_2O. A volume of 2.5 mL of protein at 2 $mg.mL^{-1}$ (HSA), 2.4 $mg.mL^{-1}$ (IgG and HRP) or 4 $mg.mL^{-1}$ (PLL) was added and the NPs were vortexed and then stirred for 1 h.

A standardized protocol was then used for the washing: the NPs were centrifuged (10,000 *g*, 10 min) and the first supernatant was collected (loading supernatant: LS). Then, the NPs were resuspended in 1 mL of dH_2O, put at rest on the block heater (25 °C, 900 rpm) for 10 min and centrifuged again (10,000 *g*, 10 min). The first washing supernatant was then collected (WS1) and the procedure was repeated once to get a second washing supernatant (WS2). Finally, the NPs were resuspended in 1 mL of dH_2O (10 $mg.mL^{-1}$).

The amount of protein was quantified using the BCA assay and the loss of NPs was taken into consideration to calculate the exact loading capacity and to correct the FWR value.

2.8. Release of protein

Two types of conditions were used here: *closed system* and *opened system*. For the *closed system*, four tubes were prepared and labelled “24 h”, “48 h”, “72 h” and “96 h”. For the *opened system*, only one tube was prepared and labelled “fresh”.

In a typical protocol, 0.2 mL of the previously prepared STMS@IBAM@Protein was transferred in a 5 mL tube (2 mg) and centrifuged (11,000 *g*, 10 min) to eliminate the supernatant prior to be resuspended in 2 mL of HEPES buffer (50 $mmol.L^{-1}$, pH 7.4). The tube was then placed on the block heater programmed to mix at 900 rpm for 24 h at 25 °C, 37 °C or 45 °C. After 24 h, the tubes “24 h” and “fresh” were centrifuged (11,000 *g*, 10 min) to collect the supernatant. The NPs in “fresh” were then resuspended in 2 mL of HEPES buffer and a new cycle of 24 h was initiated. This procedure was repeated until the tube “96 h” was collected. The supernatants were stored at 4 °C if not used immediately for quantification with the BCA assay.

2.9. Enzymatic activity

The enzymatic activity of HRP has been evaluated in dH_2O by checking its ability to catalyze the oxidation of ABTS substrate by H_2O_2. The oxidation of ABTS was monitored by recording UV–Vis spectra between 390 and 450 nm. The results were plotted using the maximum absorption at 420 nm.

In a first experiment, 1 mg of freshly prepared STMS@IBAM@HRP was resuspended in 500 μL of dH_2O in a 1.5 mL tube, which corresponded to an amount of 260.6 μg of HRP (quantified by BCA assay). Then, 500 μL of ABTS solution at 0.2 $mg.mL^{-1}$ was added, the solution was vortexed and 1.72 μL of H_2O_2 at 350 $mg.mL^{-1}$ was added (molar ratio ABTS:H_2O_2 = 1:97). The solutions were vortexed and covered with aluminium. The enzymatic activity was assessed in two different ways: for the first one, the solution was only measured by UV–vis spectroscopy

24 h, 48 h, 72 h, 96 h and 162 h after adding ABTS and H_2O_2. For the second one, 2 µL of ABTS at 50 mg.mL^{-1} and 1.72 µL of H_2O_2 at 350 mg.mL^{-1} were added to the solution to refeed it in substrate and oxidant after each UV–Vis measurement. A negative control was also prepared for both condition using only dH_2O, ABTS and H_2O_2 to monitor the natural oxidation of ABTS. All conditions were performed in duplicate.

In a second experiment, the STMS@IBAM@HRP stored in dH_2O was vortexed after 48 h of storage. The supernatant was collected in a 1.5 mL tube and the volume completed to 500 µL with dH_2O. The amount of HRP present in the supernatant was estimated using the release study results: in static conditions, 13.6% of HRP is released from the NPs, which in this case correspond to 35.4 µg of released HRP and 225.2 µg still immobilized on the NPs. The NPs were resuspended in dH_2O to have 10 mg.mL^{-1} and 1 mg were resuspended in 500 µL of dH_2O as in the previous experiment. Then, 500 µL of ABTS 0.2 mg.mL^{-1} was added and the solutions were vortexed prior to add 1.72 µL of H_2O_2 at 350 mg.mL^{-1}. The solutions were protected from light and UV–Vis spectra were collected at 1 h, 2 h, 3 h, 4 h, 5 h, 6 h, 8 h, 10 h, 24 h, 48 h, 120 h, 144 h, 168 h. A negative control containing only dH_2O, ABTS and H_2O_2 was also prepared.

2.10. Characterization methods

2.10.1. Thermogravimetric analysis

Thermogravimetric analysis (TGA) was performed on an STD Q 600 apparatus (TA instrument). The runs were performed under an air flow rate of 50 mL.min^{-1} and programmed to heat from room temperature to 800 °C with a heating rate of 5 °C.min^{-1}. TGA was used to measure the amount of organic material at the surface of STMS and thus quantify the amount of grafted APTES and IBAM. The measured weight was derived as a function of the temperature and then the curve was smoothed and integrated between 117 and 750 °C. Then, the area under the curve was used to obtain the quantity of organic material in µg of organic material per mg of STMS as in Eq. (1):

$$\text{Quantity of organic material } \left(\mu g.mg_{STMS}^{-1}\right) = 1000*\frac{\text{Area under the curve}}{m_{780°C}} \quad (1)$$

With $m_{780°C}$ the mass of material at 780°C in mg. The amount of APTES was subtracted from the total amount of organic material found after the functionalization with IBAM in order to calculate the amount of IBAM grafted on the NPs.

2.10.2. Dynamic Light Scattering and zeta potential

DLS and zeta potential were performed on a Zetasizer Nano-ZS (Malvern instruments). DLS measurements were recorded in triplicate at 25 °C and at a scattering angle of 173° using a 1 cm path length plastic cell. The measurements were conducted with a concentration of 0.2 mg.mL^{-1} of NPs in dH_2O and HEPES buffer (50 mmol.L^{-1}, pH 7.4).

Zeta potential measurements were recorded in triplicate at 25 °C using a DTS1070 folded capillary cell. The measurements were conducted in dH_2O at a concentration of NPs of 0.2 mg.mL^{-1} and as a function of pH using a titrator (MPT-2 Multi Purpose Titrator, Malvern instruments).

2.10.3. FTIR spectroscopy

FTIR spectroscopy was performed on a Spectrum Two FTIR spectrometer (PerkinElmer). First, some KBr was crushed and one drop of solution was added to it. The powder was then dried one night at 90 °C. The powder was crushed again and a press was used to obtain a KBr pellet. The spectra were obtained by the accumulation of 4 scans collected from 400 to 4000 cm^{-1} with a resolution of 4 cm^{-1}.

2.10.4. Fluorescence spectroscopy

Fluorescence spectroscopy was performed on a Fluorolog TM (Horiba Scientific) apparatus to obtain the fluorescence spectra of protein based on the fluorescence of tryptophan or of protein^{FITC} based on the fluorescence of FITC. In both case, three emission spectra were recorded and averaged by the software. The quantity of protein loaded in the particles was calculated using the quantity of free protein still present in the supernatants. A calibration curve was prepared at each experiment and for each protein and protein^{FITC}.

Protein: A 1 cm path length quartz cell was used to record the spectra from 310 nm to 500 nm with a step of 1 nm and an excitation wavelength of 295 nm. The results were plotted with the fluorescence at 337 nm.

Protein^{FITC}: A 1 cm path length plastic cell was used to record the spectra from 505 nm to 600 nm with a step of 0.5 nm and an excitation wavelength of 495 nm. The results were plotted with the fluorescence at 519 nm.

2.10.5. Bicinchoninic Acid assay (BCA)

The BCA test has been conducted using a BCA kit from Thermoscientific. In a typical procedure, a calibration curve was prepared for each protein in dH_2O in 1.5 mL tube with a volume of 500 µL for each point. Then, the supernatants were diluted adequately and prepared in triplicate (500 µL in 1.5 mL tube). The BCA solution was then prepared as indicated in the provider's protocol by mixing solution A, B and C in the proportion 50/48/2% respectively. Then, 500 µL of solution was added to each tube containing the calibration curves points and the diluted supernatants. The solutions were quickly vortexed and incubated for 1 h at 60 °C. The solutions were then cooled to room temperature using a water bath and the UV–Vis absorbance was measured (see below).

2.10.6. UV–visible spectroscopy

UV–visible spectroscopy was performed on a Lambda 950 UV/Vis spectrometer (PerkinElmer precisely) with 1 cm path length bevelled plastic cell in order to use only 1 mL of solution. It was used for the BCA assay as described above but also to monitor the enzymatic activity.

BCA: spectra collected from 560 to 570 nm with a step of 1 nm. The maximum absorption at 562 nm was used for the quantification.

Enzymatic activity: spectra collected from 390 nm to 450 nm with a step of 1 nm. The maximum absorption at 420 nm was used to plot the results.

2.10.7. Circular dichroism

The circular dichroism (CD) spectra were recorded on a J-1700 CD spectrometer (Jasco) combined with a PTC-510 Peltier thermostatted cell holder for the control of temperature (Jasco) and a 1 cm path length quartz cell with low intrinsic CD (Starna). The native HRP was dissolved in dH_2O at a concentration of 0.5 µmol.L^{-1}. The released HRP was collected after a release of 24 h in dH_2O. A volume of 1 mL of dH_2O was added to the collected 2 mL in order to fill the CD cuvette while diluting the sample the less possible. The concentration of HRP in the sample was quantified afterward using the BCA assay. The spectra were collected between 190 and 250 nm with a step of 0.2 nm, a bandwidth of 0.5 nm, a scanning speed of 5 nm.min^{-1} and a digital integration time of 2 s. Five spectra were collected and averaged for each sample.

Curve processing: the CD spectra were analyzed with the online program BestSel considering that HRP contains 308 residues (Veitch, 2004; Welinder, 1976).

2.10.8. Atomic force microscopy

2.10.8.1. Preparation of silica and silica@IBAM substrate. Several pieces of silica plate were cut (0.5 × 0.5 cm), washed with EtOH and sonicated 10 min in order to remove residues. Then, the substrates were dried with nitrogen prior to be immersed overnight in a piranha solution. This step aimed at increasing the silanol density at the substrate surface. The substrates were then washed with dH_2O and dried with nitrogen. Half of

the substrates were kept as they were and half were used for the following functionalization.

The substrates were incubated 30 min in 5 mL of EtOH, then 250 µL of NH_4OH was added and the solution stirred. A volume of 1 mL of APTES was added to the solution and the substrates were left to react 1 h 30 min. The substrates were then washed once with EtOH and twice with DMF prior to be immersed in 3 mL of DMF. A volume of 0.3 mL of Et_3N was added to the solution and the substrates were left to incubate for 5 min. Then, a solution containing 3 mL of DMF and 0.4 mL of IBC was slowly added. A white precipitate formed. The mixture was left to react overnight. Then, 1 mL of dH_2O was added to dissolve the organic salt. The mixture was stirred for 15 min to be sure that all the salt was dissolved. The substrates were then washed three times with DMF and one time with EtOH prior to be dried with nitrogen. All substrates were stored in a closed plastic box.

2.10.8.2. Functionalization of AFM tips. AFM tips were functionalized with HSA or HRP *via* a 6 nm-long acetal-PEG linker according to the protocol published by Hinterdorfer and Dufrêne (Hinterdorfer and Dufrêne, 2006) and Francius et al.(Francius et al., 2009). All the glassware was washed with piranha solution, then with NaOH 4 $mol.L^{-1}$, dH_2O and EtOH prior to be dried with nitrogen to remove all possible pollutants.

Amino-functionalization of AFM tips. A solution containing 3.3 g of ethanolamine hydrochloride and 6.6 mL of DMSO was prepared in a reactor by heating it at 60 °C. The solution was left to cool down after complete dissolution. A molecular sieve was placed at the bottom of the reactor as well as a Teflon plate. The cantilevers (MLCT, non-conductive silicon nitride, Bruker) were washed in $CHCl_3$ (3 × 5 min) and dried with nitrogen prior to be immersed in the ethanolamine hydrochloride solution. The reactor was closed and the cantilevers were incubated overnight. The cantilevers were washed with DMSO (3 × 1 min) and EtOH (3 × 1 min) prior to be dried with nitrogen.

Functionalization of the AFM tips with an acetal linker and with proteins. A small reaction chamber was placed in a new reactor and surrounded by a molecular sieve. A portion of 1 mg of acetal-PEG-NHS was dissolved in 0.5 mL of $CHCl_3$ and transferred into the reaction chamber. Then, 30 µL of Et_3N was added and the solution was mixed. The cantilevers were immersed in the solution, the reaction chamber closed and left to react for 2 h. The cantilevers were then washed with $CHCl_3$ (3 × 10 min) prior to be dried with nitrogen. The cantilevers were immersed for 10 min in citric acid 1%, washed with dH_2O (3 × 5 min) and dried with nitrogen prior to be placed on a Teflon plate. Then, 100 µL of a 0.2 $mg.mL^{-1}$ protein solution was pipetted onto the cantilevers and 2 µL of a 1 $mol.L^{-1}$ sodium cyanoborohydride (32 mg $NaCNBH_3$, 50 µL of NaOH 20 $mmol.L^{-1}$ and 450 µL of dH_2O) was added and mixed by up-and-down movement. The Teflon plate was covered to be protected from dust and left to react for 1 h. Then, 5 µL of a 1 $mol.L^{-1}$ ethanolamine solution (pH 8) was added and mixed into the solution. The cantilevers were left to incubate for 10 min and then washed with dH_2O (3 × 5 min).

2.10.8.3. Measurement. AFM force spectroscopy was performed on a Bioscope Resolve (Bruker France SAS, Palaiseau, France) apparatus using Nanoscope software (Bruker) at room temperature in dH_2O. The experiment was conducted using HSA or HRP-functionalized tips both on silica surface and silica@IBAM surface. For each combination protein/substrate, a force map was recorded on a 5 × 5 μm^2 surface corresponding to 32 × 32 points (1024 curves). The hold time was fixed at 100 ms.

2.10.8.4. Curve processing. For each AFM force measurement, a force map containing 1024 force curves was obtained and analyzed by Nanoscope analysis (Bruker). Retraction curves were analyzed to determine the number of adhesive events (negative peaks) corresponding to the force of interaction between each couple protein/substrate. Statistical analysis were performed on the number of detected peaks on each retraction curve and also on the intensity of the peak characteristic of the interaction protein/substrate which represents the required force to break the protein/substrate interaction.

3. Results and discussion

3.1. Synthesis and functionalization of STMS with IBAM groups

The synthesis of STMS has been done as reported previously (Bizeau et al., 2021; Duenas-Ramirez et al., 2020; Perton et al., 2019a). Briefly, the NPs were synthesized using the sol-gel method in presence of CTATos as surfactant in order to obtain a stellate morphology, based on the work reported by Zhang et al. (Zhang et al., 2013a). A TEM image is presented in Fig. S1.A and shows that the NPs display the expected stellate morphology. The STMS diameter and the statistical analysis obtained from these TEM images are presented in Fig. S1.B and give a mean diameter value of 124 ± 27 nm. The STMS were then functionalized with APTES using the siloxane condensation reaction in order to add amines on the NPs surface and the IBAM groups were then formed at the NPs surface by reaction of the amino groups with the acyl chloride IBC. The hydrodynamic diameter measured by DLS and the zeta potential measurements of STMS, STMS@APTES and STMS@IBAM presented in Fig. S2.A and S2.B show that the suspension of the particles was stable with a zeta potential switching from negative for STMS (−20 ± 0.6 mV) to almost zero with APTES (−0.7 ± 0.2 mV) and then to positive with IBAM (34.7 ± 0.6 mV). The FTIR spectra (Fig. S2.C and Table S1) show the specific peaks of the amide bond formed after the reaction with IBC, bringing confirmation about the chemical IBAM functionalization of the NPs surface. The amount of APTES and IBAM grafted on the STMS were determined by thermogravimetric analysis (TGA). A representative TGA curve is given in Fig. S3.A and the curves used for the calculation in Fig. S3.B. The amount of organic material (APTES+IBAM) was determined to be 242 ± 55 $\mu g.mg^{-1}$ STMS in average, which is in agreement with previous experiments, meaning that the grafted amount of IBAM is *ca.* 131 $\mu g.mg^{-1}$ STMS which represents *ca.* 2.3 IBAM/nm^2 (Bizeau et al., 2021; Duenas-Ramirez et al., 2020).

3.2. Loading of proteins and characterization of STMS@IBAM@Protein

The first step of this work was to study the loading of proteins in the STMS@IBAM NPs. To do so, the amount of NPs was fixed and the amount of protein in the loading solution was progressively increased following the FWR defined by Eq. (2):

$$FWR = 100 * \frac{m_{added\ protein}}{m_{STMS}} \quad (2)$$

Then, to measure the amount of loaded proteins within the NPs, we used the indirect quantification method consisting in measuring the amount of remaining protein in the loading supernatant (LS). At this point, a challenge was to choose the right detection technique to perform our measurements.

Indeed, although detection kits are developed since years in order to answer this problem, the quantification of proteins is not a facile and routine task, and scientists still encounter problems when performing such measurements. Such difficulties come from the combination of several parameters: the amount of protein available for the assay (sensitivity), the composition of the sample (interferences), the amino-acid sequence of the protein (sensing specificity) and how tests are used and reported (operator). As an example, Zaguri et al. identified 19 distinct methods to quantify proteins used by ecologists, and they notably noted the variability of how a given method can be used (difference in the incubation time, temperature…) and how the protocol can be reported (Zaguri et al., 2021). To give a precise example, they found that only 8% of the studies using the Bradford assay in their corpus

reported the incubation time, and only 5% reported the incubation temperature. They also experimentally showed the influence of protocol variations on the results. Knowing that, and knowing that all assays cannot be used with all proteins or that some assays are very sensitive to the composition of the sample (presence of salts, buffer, detergents etc), the choice of the adequate technique is already a challenge *in* the challenge of quantifying proteins. Some authors proposed decision-making flow charts to help researchers select the most adequate technique, taking into account the sample and the buffer compositions (Noble and Bailey, 2009; Olson and Markwell, 2007). However, these flow charts often give several assays for a given sample.

Thus, some authors prefer to use several techniques, either to check which one is the most appropriate by using them on a known sample (Knight and Chambers, 2003) or to obtain the more accurate value for their measurement (De Mey et al., 2008). Last but not least, the preparation of the calibration curve is a key aspect of protein quantification. Bovine serum albumin is the most commonly used protein for the calibration curve, which was explained by Stoscheck in 1990 by the fact that it is inexpensive, easy to use and was so much used that comparison is easy to do between previously reported and newly generated values (Stoscheck, 1990). IgG was also reported to be used as a standard protein, but to a less extent. However, Stoscheck already warned the community that all proteins do not react in the same way in each assay, due to their secondary and tertiary structure and their environment sensitivity, and that the protein that is aimed to be quantified should be used for the calibration curve also. At least, the standard protein should be close to the quantified protein, as reminded more recently by Knight and Chambers (Knight and Chambers, 2003). Also, it is important to understand well how tests work to evaluate if the calibration curve has to be done at each quantification or not. For instance, in the Lowry assay (Olson and Markwell, 2007), the calibration curve has to be repeated at each experiment to ensure that the amount of protein would not be under- or overestimated by a change in the reaction time.

Taking all this information into account, we decided to use three complementary detection techniques based on fluorimetry or UV–Vis spectrometry. By doing so, we could investigate the reliability of the different quantification methods to estimate the loaded and released proteins, determine their relevance with a given protein and achieve a more precise quantification. In addition, we performed a calibration curve for each experiment, using all proteins as their own standard protein. In a first technique, the proteins were labelled with FITC and the fluorescence of the bound FITC group was measured. In a second technique, the intrinsic fluorescence of proteins due to the tryptophan residue was exploited. This fluorescence is due to only one tryptophan residue that can be found in the structure of HSA (Maciążek-Jurczyk et al., 2018; Meloun et al., 1975) and HRP (Welinder, 1976). Regarding IgG, it has been reported that the heavy chain contains in average 7.5 tryptophan residues and the light chain 2.3 tryptophan residues. Thus, IgG contains around 19.6 tryptophan residues, as this antibody is composed of twice each chain and depending the IgG subclass used (Chaplin et al., 1965; Papadea and Check, 1989). These two techniques are very easy to set but the FITC and tryptophan fluorescence can be influenced by their environment such as pH or protein conformation (Chen and Barkley, 1998; Klugerman, 1965; Vivian and Callis, 2001). Thus, the third technique used was aimed at avoiding such environment-dependency, so the BCA assay was chosen as it uses the ability of peptide bonds in proteins to reduce Cu^{2+} in Cu^{+}. The obtained Cu^{+} then forms a complex with two BCA molecules to form a purple metallic complex detectable by UV–Vis spectroscopy (Smith et al., 1985; Walker, 2009). Once the amount of unloaded protein was measured, the amount of loaded protein was calculated as well as the loading capacity (LC) of the NPs defined as in Eq. (3):

$$\mathrm{LC}\ \left(\mu\mathrm{g.mg^{-1}}\right) = \frac{m_{\text{loaded protein}}}{m_{\text{STMS}}} = \frac{m_{\text{added protein}} - m_{\text{protein in LS}}}{m_{\text{STMS}}} \quad (3)$$

with $m_{\text{loaded protein}}$ in µg and m_{STMS} the mass of unmodified STMS in mg.

The calibration curves for each protein and each technique are presented in Fig. S4, S5 and S6 and the protein loading results as a function of the FWR are presented in Fig. 1. A good correlation between the three detection techniques can be seen for HSA and HRP, with a maximum LC as high as *ca.* 670 ± 7 µg.mg^{-1} for HSA (Fig. 1.A) and *ca.* 396 ± 10 µg.mg^{-1} for HRP (Fig. 1.B) (BCA assay values). However, for IgG, Fig. 1.C shows a huge difference between the LC evaluated with the fluorescence of FITC as compared to the two other techniques: a maximal LC of *ca.* 557 ± 101 µg.mg^{-1} was detected with IgG^{FITC} while the maximum was only *ca.* 261 ± 148 µg.mg^{-1} with the fluorescence of tryptophan and *ca.* 166 ± 22 µg.mg^{-1} with the BCA assay. Even if we do not have a direct proof of it, we suppose that some local effect could have lowered the FITC signal and thus underestimate the amount of IgG^{FITC} in the LS. As the fluorescence of tryptophan and the BCA assay were giving similar results, we considered these values as the most likely ones. Regarding PLL, only PLL^{FITC} is given in Fig. 1.D and shows a maximum LC of *ca.*71 ± 10 µg.mg^{-1}, which is quite low as compared to HSA and HRP. Even if the BCA assay has been reported for this molecule in the literature (Higuchi et al., 2006; Shitole et al., 2020; Wang et al., 2018; Wu et al., 2017b), it was tried on three different batches and did not show reliability here. Hence, this first study clearly shows how tricky it can be to quantify proteins and the usefulness of several concomitant techniques to be sure that all the loading results converge to the same value. In addition, it also showed that the STMS@IBAM was able to load large amounts of HSA and HRP as compared to IgG and PLL. For the rest of the study, a working FWR of 71% of HSA (592 ± 3 µg.mg^{-1} LC), 85% of HRP (396 ± 10 µg.mg^{-1} LC) and IgG (103 ± 5 µg.mg^{-1} LC) and 142% of PLL (71 ± 10 µg.mg^{-1} LC) were chosen as they lead to high and optimal LCs for each protein. If nothing is precised, the label STMS@IBAM@Protein used in the following sections refers then to these formulations.

The colloidal stability of STMS@IBAM@Protein NPs was then evaluated in dH_2O for all proteins. As it can be seen in Fig. 2, the NPs form stable colloidal suspension in dH_2O with all proteins, with mean hydrodynamic diameters of 180 and 151 nm for HSA and HRP respectively. The mean hydrodynamic diameters of STMS@IBAM@IgG and STMS@IBAM@PLL were higher, 220 and 340 nm respectively, which make them less interesting for biological applications as they may aggregate or rapidly be identified by the immune system. In addition, the isoelectric points (IEPs) of 5.5 for STMS@IBAM@HSA, and 6.2 for STMS@IBAM@HRP ensure that these particles would be negatively charged in biological conditions (pH 7.4), while the IEP of STMS@IBAM@PLL at 8.3 means that these NPs would be mainly positively charged. HSA- and HRP-loaded NPs are thus of greater interest as negatively charged particles are less prone to opsonisation and macrophages uptakes (Alexis et al., 2008). Regarding IgG, the IEP at 7.4 means that the NPs would be neutral in biological conditions, which was reported to also reduce NP clearance by phagocytosis (Alexis et al., 2008). However, unless they have a suitable steric hindrance, neutral particles may aggregate, which is not desirable for medical application.

The aim of this work was not only to study the STMS@IBAM as an anchoring surface for the loading of proteins but also to evaluate its ability to deliver them through sustained release for medical application. Given the issues to quantify PLL and IgG by convergent detection techniques seen above, and the colloidal stability study of the STMS@IBAM@Protein NPs, we will focus only on STMS@IBAM@HSA and HRP as suitable systems to investigate in the next sections the chemical engineering aspects (3.3), the sustained protein release (3.4) and force-surface interactions (3.6).

3.3. Chemical engineering aspects

As a preliminary and prerequisite study to prepare samples for sustained protein release, we investigated the possibility to scale-up the protein loading process as well as the stability of the loading (spontaneous leaking) over consecutive washings.

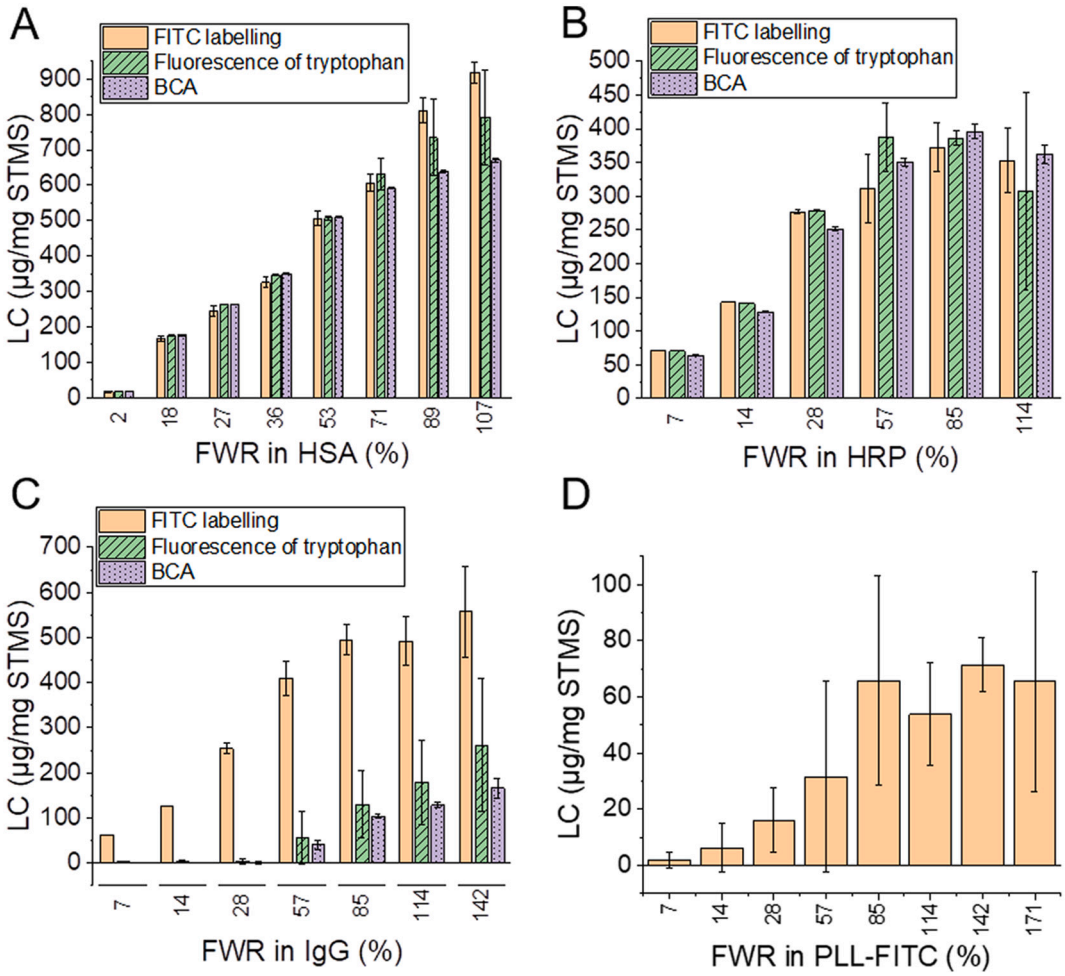

Fig. 1. Loading of A) HSA, B) HRP, C) IgG and D) PLL^{FITC} on STMS@IBAM in function of the protein FWR.

In the objective of using these NPs as PDS for medical application, it is important to be able to produce a relatively high amount of NPs. Thus, a scale-up study was performed with the aim to move from mg to the ten mg-range scale. A schematic representation of the scale-up applied to each system is given in Fig. 3.A: it consisted in multiplying the masses and volumes by 2.5 and 5 for HSA and HRP respectively and keeping the incubation time at 1 h. The comparison of the LC obtained by the as above-described BCA assay before and after the scale-up is given in Fig. 3.B and .C. These graphs show that the scale-up had a very low impact on the LC of HSA as it was reduced by only 18%. Regarding HRP, the impact was quite higher as the LC was reduced by 33%, maybe due to the fact that the loading time was kept at 1 h while all the rest of the conditions were multiplied by five. However, the obtained LC (*ca.* 264 $\pm$ 3 µg.mg^{-1}) was still interesting for protein release applications. Thus, the label STMS@IBAM@Protein will correspond to a STMS@IBAM NPs containing 484 $\pm$ 3 µg.mg^{-1} of HSA or 264 $\pm$ 3 µg.mg^{-1} of HRP for the release study. It has to be noted that the LC obtained after the scale-up is the average obtained from 12 to 13 batches, showing a very good reproducibility of the protein loading process (showed in Fig. 3 D and E).

As the NPs are dedicated to medical applications, it is important to eliminate any possible pollutant of the process or loosely bound proteins by several washings. Thus, a standardized washing protocol was implemented prior to protein release and protein leaks were quantified (see Fig. S7). Results show that small fractions of proteins are lost upon two consecutive washings ($\leq$8 wt% in total).

3.4. Protein release study

Then, the release of proteins from the STMS@IBAM NPs was studied in HEPES aqueous buffer (50 mmol.L^{-1}, pH 7.4), to better mimic biological conditions, and considering two different conditions called *closed* or *opened systems*. The *closed system* mimics a static condition of protein release where the particles are kept in the same aqueous solution over the studied period (four days) and thus where an equilibrium is established. Conversely, the *opened system* mimics a dynamic aqueous flow where the aqueous solution is changed every 24 h during the period, displacing the equilibrium every day. The protein release was also investigated at 25, 37 and 45 °C in order to get insights on the release profiles at respectively a preparation temperature, the human biological temperature and a characteristic temperature of magnetic hyperthermia. Indeed, iron oxide NPs with controlled size and shape are good heating agents under magnetic stimuli (among other stimuli) (Cotin et al., 2018) and the addition of a stellate silica shell around these iron oxide NPs was already reported and showed good heating properties too (Adam et al., 2021; Perton et al., 2019b). Thus, a combination of this magnetic core and our protein loaded-STMS shell could be considered to couple different therapeutic effects in a single nanocarrier. The STMS@IBAM@Protein were thus resuspended in HEPES buffer and the NPs colloidal stability was checked and showed good results (see Fig. S8) as previously in dH_2O.

The *closed system*, schematically represented in Fig. 4.A, consisted in reproducing static conditions where the STMS@IBAM@Protein NPs are dispersed in the aqueous HEPES buffer during a given period in equilibrium conditions. Thus, to achieve this study, 5 mL tubes were

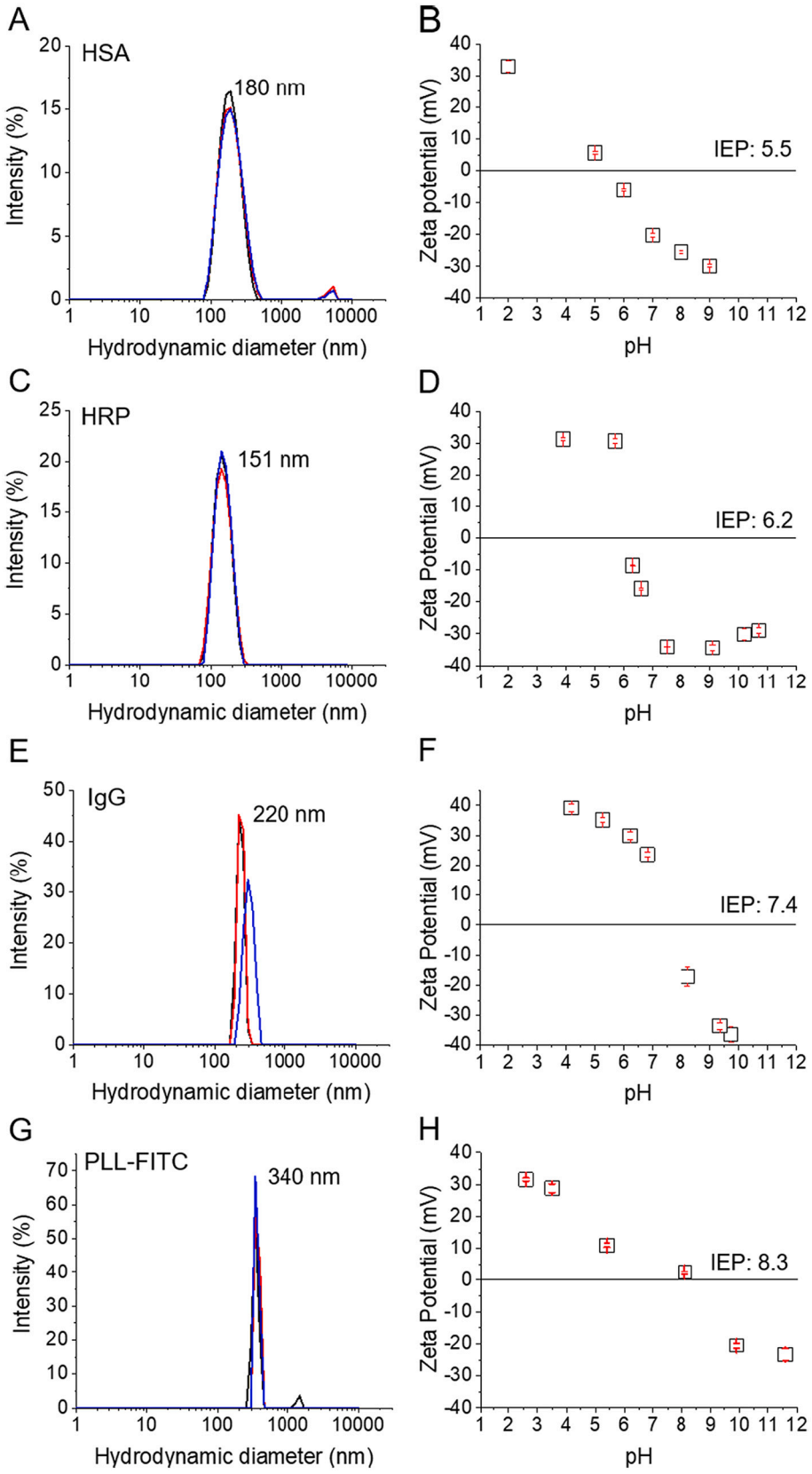

Fig. 2. Colloidal stability in dH_2O. DLS measurements (triplicates) and zeta potential as a function of pH for STMS@IBAM@HSA (A) and B) and respectively), STMS@IBAM@HRP (C) and D) respectively), STMS@IBAM@IgG (E) and F) respectively) and STMS@IBAM@PLL^{FITC} (G) and H) respectively).

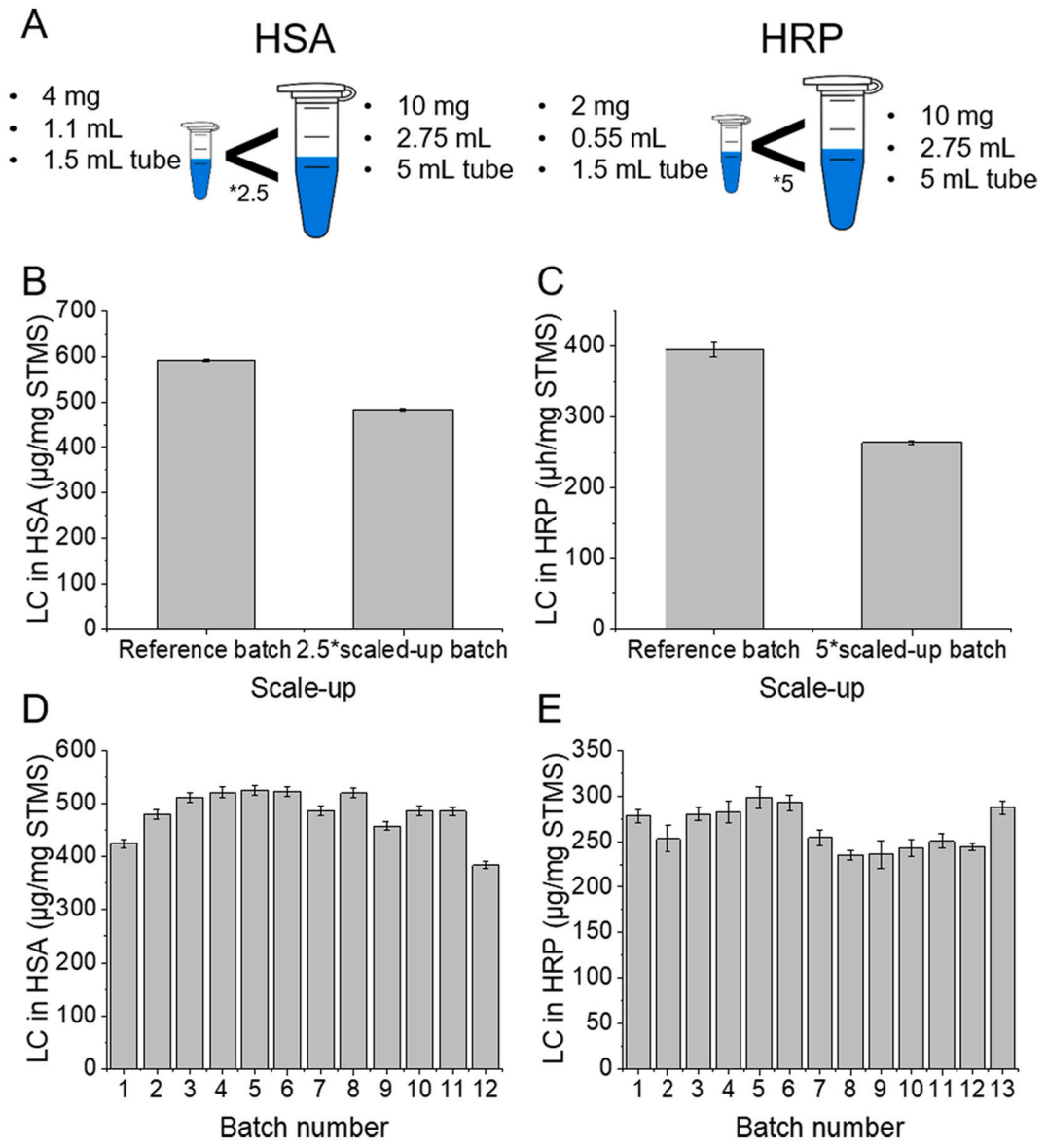

Fig. 3. A) Schematic representation of the scale-up study operated for each protein. Comparison of the LC obtained before and after the scale-up for B) HSA and C) HRP. Reproducibility of the loading of D) HSA and E) HRP on STMS@IBAM after the scale-up.

prepared for each time point (24, 48, 72, 96 h), meaning that the NPs were in solution during all the corresponding time. The cumulative release obtained for HSA and HRP are presented in Fig. 4.B and .C respectively. In both cases, no influence of the temperature could be seen. Also, a burst release of *ca.* 28 ± 0.3% for HSA and *ca.* 14 ± 0.2% for HPR can be observed during the first 24 h, but then, the amount of protein in solution does not increase anymore over time. Such a diffusion profile could mean that the system has already reached an equilibrium at 24 h and that no more protein can be desorbed in the system if left as it is. The application of mathematical models on the data suggests that a Fickian diffusion would drive the release in this condition (see the Supporting Information S9, Fig. S9 and Table S2 and S3 for more details) which is in agreement with the fact that once an equilibrium is reached, no more protein is released.

The *opened system*, schematically represented in Fig. 5.A, consisted in mimicking, as a first approximation, the dynamic conditions than NPs would encounter when administered as a therapeutic treatment. To do so, only one 5 mL tube was prepared and the buffer was collected and replaced every 24 h. The results are presented in Fig. 5.B for HSA and .C for HRP. Here again, no influence of the temperature could be seen. However, unlike the results obtained in the closed systems, what can be observed here is that the release of proteins was continuous after the first 24 h burst release. Indeed, an average linear release of 6.4% per 24 h and 8.4% per 24 h were observed for HSA and HRP respectively. This continuous release is a very good result for therapeutic application as it means that the proteins would be released slowly over time in a sustained way. Here also, mathematical models were applied to the data to estimate the possible mechanism involved in the release (see the Supporting Information S9, Fig. S9 and Table S2 and S3 for more details). The results suggest that the release of HSA in this *opened* condition would also be driven by Fickian diffusion while the release of HRP would be attributed to a mix of diffusion and eventually erosion of the NPs. Indeed, it has been shown these last decennia that silica NPs can degrade in various physiological media such as phosphate-buffered saline (PBS), fetal bovine serum (FBS) or even Dulbecco's modified Eagle's medium (DMEM), among the reported media (Chen et al., 2015; Croissant et al., 2017; Hao et al., 2012; Möller and Bein, 2019). Thus, it is not excluded that in our dynamic condition, some slight silica degradation would happen and then would participate in the release of proteins. Especially in the case of HRP which has a half quantity

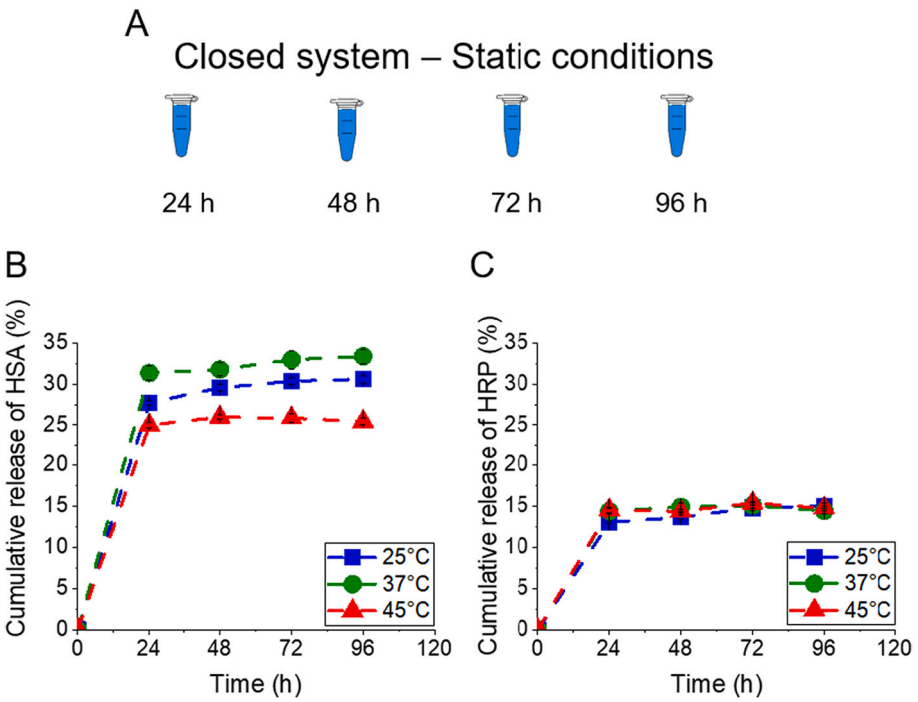

Fig. 4. A) Schematic representation of the closed system used for the release. Cumulative release in closed system of B) HSA and C) HRP.

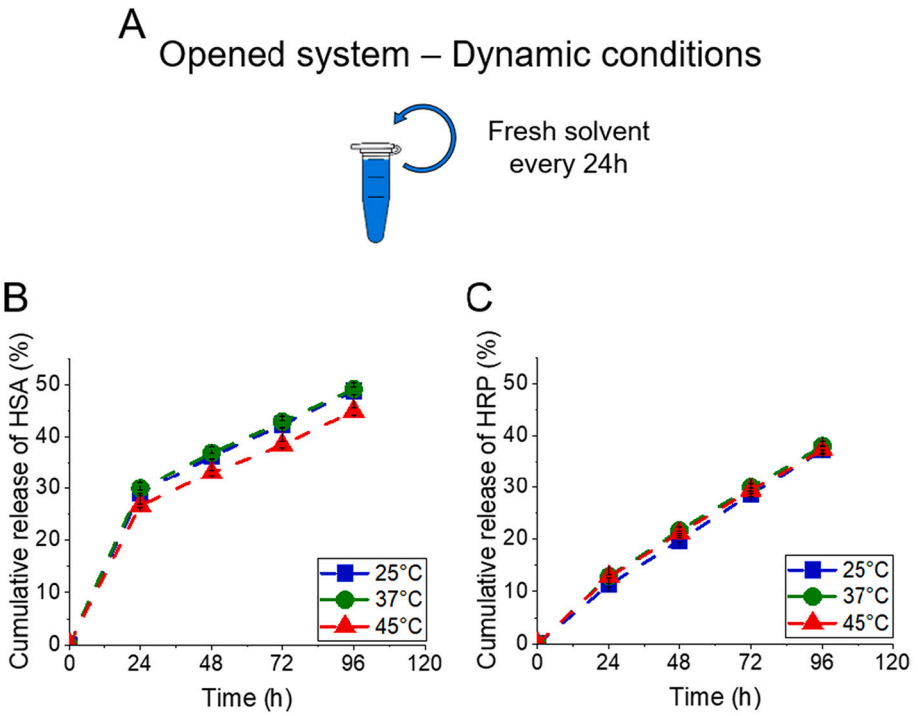

Fig. 5. A) Schematic representation of the opened system used for the release. Cumulative release in opened system of B) HSA and C) HRP.

adsorbed on STMS@IBAM as compared to HSA, the layer of HSA may protect the NPs from erosion longer than the HRP.

3.5. Enzymatic activity of immobilized and released HRP

One important element to check when releasing proteins through PDS is that their activity is retained despite the loading and release processes. Thus, the enzymatic activity of HRP was monitored using the ABTS substrate and H_2O_2, as the bio-catalytically obtained radical cation $ABTS^{+\bullet}$ is green and can be detected by UV–Vis spectroscopy.

A first experiment was to investigate the biocatalytic activity of HRP when it is immobilized on STMS@IBAM. Hence, freshly prepared STMS@IBAM@HRP NPs were incubated with ABTS and H_2O_2 with or without a daily feeding in ABTS and H_2O_2. The amount of HRP was measured to be 260.6 μg and a molar ratio ABTS:H_2O_2 of 1:97 was chosen. The same amount of ABTS and H_2O_2 were added every 24 h in the "daily feeding" condition. The control experiment was the natural oxidation of ABTS in presence of H_2O_2 without any HRP in the solution

(and without NPs). The results are presented in Fig. 6.A. First of all, it is noticeable that the control shows only a very negligible natural oxidation of ABTS when the solution is daily fed in ABTS and H_2O_2 (dark blue, round symbols). Also, no oxidation could be seen when the solution was not refed (pale blue, cubic symbols). Then, regarding the STMS@IBAM@HRP NPs incubated with ABTS and H_2O_2, the simple mix of NPs with the reactants (pale yellow, cubic symbols) shows that the immobilized enzyme-induced oxidation occurs mainly during the first 24 h but with a low continuous activity during the next days. Nonetheless, when the solution was refed (dark yellow, round symbols), the signal kept increasing in a clear way, meaning that a great amount of ABTS was converted every 24 h, and thus meaning that the HRP kept its activity over time.

In a second test, we aimed at comparing the activity of the released HRP to the activity of the immobilized HRP. To do so, the supernatant was collected after 48 h of storage and completely used for the biocatalytic study. The amount of HRP in the supernatant was estimated to be 35.4 µg using the results obtained in the release study (see the materials and methods section for more details). The amount of remaining HRP on the STMS@IBAM was thus calculated to be 225.2 µg. The results presented in Fig. 6.B show that both released HRP and immobilized HRP

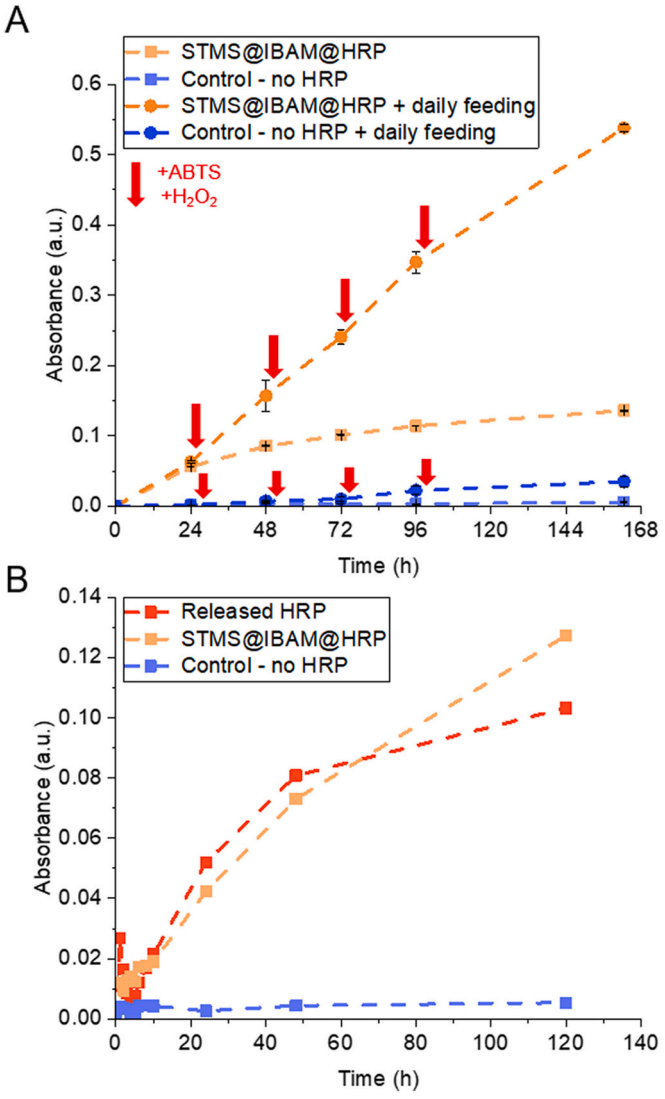

Fig. 6. A) Enzymatic activity of HRP immobilized on STMS@IBAM with and without daily feeding in substrate and oxidant. B) Comparison of the enzymatic activity of HRP released from STMS@IBAM and immobilized on STMS@IBAM.

are active, and have similar catalytic conversion levels while the amount of immobilized HRP is *ca.* 6 times more as compared to released HRP. This indicates that enzymatic activity is quite affected by the immobilization on the NPs and is increased when released in buffer.

Altogether, the enzymatic activity experiments showed that the HRP is able to catalyze the oxidation by H_2O_2, whether released from or still immobilized on the NPs.

As the conformation of protein is an important parameter that ensure their biological properties, we investigated it by performing circular dichroism spectroscopy on the native and released HRP and by extracting their secondary structure using the online program BestSel (Micsonai et al., 2021; Micsonai et al., 2018; Micsonai et al., 2015). The graphs presented in Fig. S10.A show a profile similar to what is expected for proteins containing mainly α-helix, as reported by Greenfield and Fasman (Greenfield and Fasman, 1969). The analysis of the secondary structure (Fig. S10·B-D) confirms it, but also show a difference between the native and the released HRP (lower amount of α-helix and higher amount of β-sheet in the released HRP). Thus, the loading and release processes has an impact on the HRP conformation, but results only in a reduction of its enzymatic activity, keeping its bio-functionality and interest as a PDS.

Up to now, this study showed the interest in using STMS@IBAM NPs to load and to deliver proteins in a sustained way when submitted to dynamic conditions. While HSA and HRP have similar properties in terms of molecular weight _ 66,478 and 40,000 $g.mol^{-1}$ respectively – and IEP - 4.7 for HSA (Carter and Ho, 1994) and 4.8 for HRP (see Fig. S11) their levels of adsorption (maximum 670 ± 7 $\mu g.mg^{-1}$ for HSA *versus* 396 ± 10 $\mu g.mg^{-1}$ for HRP) and release (48 ± 0.5% for HSA *versus* 37 ± 0.4% for HRP, dynamic conditions) were found quite different and protein-dependent. In a last section of this work, we attempt to decipher and quantify the interactions involved between IBAM surface and each of the two proteins through AFM-force study on planar substrates (silicium-SiO_2@IBAM surface). The results are compared to the interactions involved in the absence of IBAM groups (bare silica surface).

3.6. *Protein-surface interactions: AFM-force measurements*

Hence, in this section, with the aim to provide some quantitative insights in the interactions of proteins with IBAM groups at the protein scale, an AFM spectroscopy study in the force mode was used. AFM is renown as a powerful tool that allows to better understand physical interactions between two elements at nm- and even sub-nm scales (Cappella and Dietler, 1999; Janshoff et al., 2000). The principle of this technique has been represented and explained in Scheme S1. Briefly, HSA or HRP were covalently conjugated to the AFM tip using a PEG-acetal linker. The protein-attached AFM tip was then used to sense the local force at play between the proteins and planar substrates. To emphasize the input of IBAM surface chemical modification, interactions of proteins with silica@IBAM (Si-SiO_2-IBAM) were compared to bare silica (Si-SiO_2, a silicon chip with a natural passivated SiO_2 layer).

The first analysis performed on the obtained force map (1024 curves) was a statistical analysis on the number of peaks present in each curve (Fig. S12). This analysis showed that the protein/substrate interaction was mainly broken with limited unfolding of the protein, as the curves presented only one peak in 85 to 97% of the cases. However, it can be noted that 11% of the curves presented two peaks in the case of HSA/SiO_2-IBAM, meaning that some unfolding could happen in few cases for this couple.

Then, the statistical analysis on the force was performed and the results are presented in Fig. 7.A (HSA) and .B (HRP). In the case of HSA, it appears that there are more interactions between HSA and SiO_2-IBAM than between HSA and SiO_2, as only *ca.* 0.6% of the curves in the HSA/SiO_2-IBAM force map showed no peak against *ca.* 76% in the HSA/SiO_2 force map. Adhesion force histograms indicate that the main adhesion force was determined at 137 ± 51 pN for HSA/SiO_2 (with some cases at

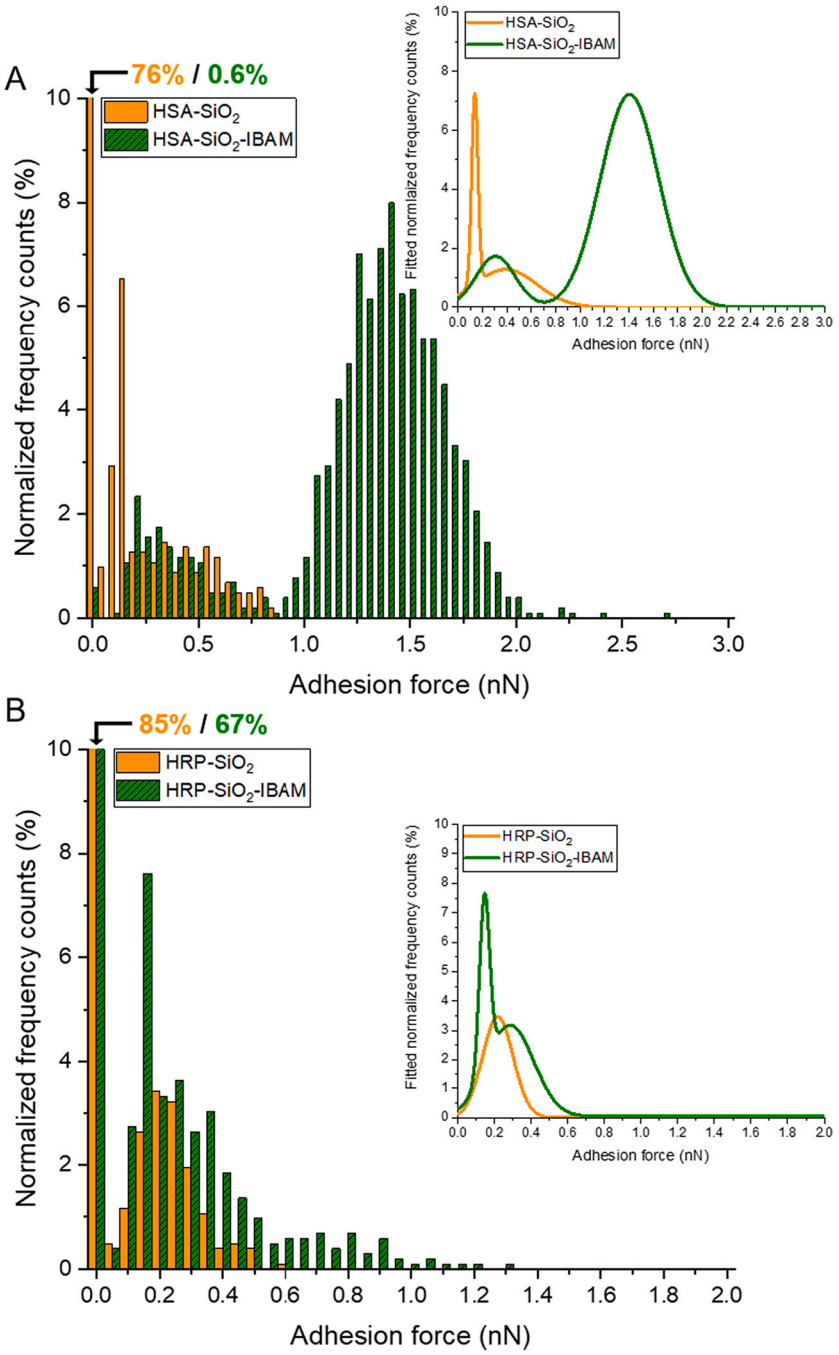

Fig. 7. Adhesion force histograms obtain with AFM force on SiO_2 or SiO_2-IBAM surface for A) HSA and B) HRP. Insets represent the fitted curves obtained from the histograms.

389 ± 515 pN) while the main adhesion force for HSA/SiO_2-IBAM was at 1400 ± 478 pN (with some cases at 308 ± 321 pN) (Fig. 7.A). These values clearly show that the interactions between HSA and IBAM are of intermolecular nature and are stronger than between HSA and SiO_2.

Regarding HRP, the results shown in Fig. 7.B lead to quite different conclusions. Indeed, first, *ca.* 85% and *ca.* 67% of the curves showed no peak for the HRP/SiO_2 and HRP/SiO_2-IBAM respectively, meaning that there are few interactions between HRP and the two surfaces, with a low preference with the IBAM-functionalized substrate. Second, as it can be seen in the inset, the main adhesion forces were also quite similar, as it was *ca.* 217 ± 167 pN for HRP/SiO_2 and *ca.* 145 ± 55 pN and 286 ± 255 pN for HRP/SiO_2-IBAM. Altogether, these results show that the interaction between HRP and IBAM is not much higher than with SiO_2.

Complementary to the AFM study, we have compared the loading contents of HSA and HRP on bare STMS and STMS@IBAM in the exact same loading conditions. Considering the IEPs of HSA and HRP, the proteins are thus mainly negatively charged in these conditions, like the STMS NPs, while the STMS@IBAM NPs are positively charged. The results presented in Fig. 8.A show that the loading of HSA was much more efficient when functionalizing the NPs with IBAM, as the LC was only *ca.* 120 ± 9 $\mu g.mg^{-1}$ on STMS and *ca.* 443 ± 31 $\mu g.mg^{-1}$ on STMS@IBAM. However, in the case of HRP, the LC was quite similar on both surfaces: *ca.* 219 ± 7 $\mu g.mg^{-1}$ on STMS and *ca.* 271 ± 8 $\mu g.mg^{-1}$ on STMS@IBAM (Fig. 8.B). At any point, and considering that the force of interactions found by AFM can be correlated to the protein loading extent, both studies tend to similar results in terms of force adhesion and protein

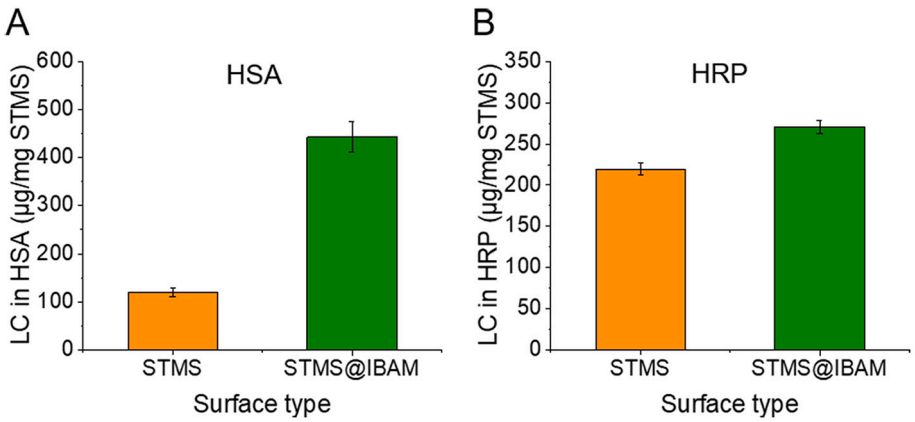

Fig. 8. Comparison of the LC of A) HSA, B) HRP on STMS and STMS@IBAM.

adsorption.

These both analysis (AFM and protein loading studies) not only give us information about the difference of interactions between a protein and the two substrates (IBAM *vs* BARE), but they also give insights on the types of interactions involved between the adsorbed protein and these substrates. Indeed, it has been reported that forces measured by AFM are usually *ca.* 60 pN for van der Waals interactions, *ca.* 200 pN for hydrogen bonds (H-bonds) and *ca.* 650 pN for hydrophobic interactions which provide us a kind of scale-force to interpret results in term of intermolecular interactions (Cappella and Dietler, 1999). Specific interactions between an antibody and its antigen were also studied and can give values up to 340 pN (streptavidin/biotin (Janshoff et al., 2000)).

In our case, the obtained values when HSA (137 ± 51 pN) and HRP (217 ± 167 pN) proteins are in contact with the bare SiO_2 substrate suggest that the main interactions involved between the silanols groups of SiO_2 and the polypeptide chains of proteins correspond to H-bonds. This result is also supported by the non-negligible loading of these two proteins on bare STMS (12 wt% for HSA and 22 wt% for HRP) despite the repulsive electrostatic interactions occurring between STMS and the proteins.

Regarding the interactions of the tip-attached proteins with SiO_2-IBAM substrate, the AFM and protein loading studies show that HSA and HRP have different behaviours.

The value in the range [145–286] pN obtained for HRP in contact to SiO_2-IBAM substrate strongly suggests that H-bonds interactions occur also between the IBAM bonds and the proteins with a similar level than the silanols of the bare substrate. The close loaded amounts of HRP measured on STMS@IBAM as compared to STMS (27 *vs* 22 wt%) are also in agreement with a protein loading mediated by such H-bond interactions. Interestingly, while the interaction of silica@IBAM with HRP is favourable in terms of surface charge, the electrostatic forces do not seem to contribute here to the protein binding.

Regarding now the noticeable high value of 1400 ± 478 pN measured in the couple HSA/SiO_2-IBAM, and taking into account favourable electrostatic charges of HSA and silica-grafted IBAM, it is not excluded that this huge adhesion force value results from a combination of intermolecular forces: H-bonds, electrostatic forces and even hydrophobic interactions. Indeed, regarding hydrophobic aspects, it is well known that HSA possesses hydrophobic pockets in his two subdomains IIA and IIIA and that theses pockets are the principal binding sites of the protein for a broad range of molecules (He and Carter, 1992; Kumari et al., 2014; Shahabadi et al., 2013; Trynda-Lemiesz, 2004). Hydrophobic interactions may thus happen between HSA and the terminal methyl groups of IBAM. It can be noted that the ability of HRP to form hydrophobic bonds was also demonstrated in the literature, and it is even suggested that the hydrophobic "patch" due to three phenylalanine groups is involved in the binding of substrates near the heme region of this protein (Gajhede et al., 1997; Huang et al., 2018; Schejter et al., 1976; Zhang et al., 2012). However, the value obtained in our study does not allow us to think that such interactions occur here, highlighting again the different behaviour between HSA and HRP. At last, the higher loading value amount of HSA measured on STMS@IBAM as compared to STMS (44 *vs* 12 wt%) underlines the association of these three favourable interactions helping the protein loading. HSA could thus be adsorbed on a higher quantity on the STMS@IBAM NPs thanks to the different types of interactions involved in the process.

Furthermore, the latter point would also explain the different amounts of protein released when the STMS@IBAM@Protein are incubated in a buffer at physiological pH (7.4) in Figs. 4 and 5. At this slightly higher pH, it is hypothesized that the electrostatic interactions between HSA and IBAM would be reduced due to the decrease of the IBAM charge, leading to the observed burst release of 28% of HSA, which is the double of the one observed for HRP. As described above for HRP, the electrostatic interactions would not play a role in the protein release.

4. Conclusion

In this study, a specific attention was given to the loading and sustained release of various proteins from STMS@IBAM NPs.

Thus, the rigorous quantification of proteins and polypeptide (HSA, HRP, IgG, PLL) was achieved by combining three different quantification techniques (FITC labelling, intrinsic tryptophan fluorescence and BCA assay) to evaluate precisely the protein loading capacities as a function of the FWR. This work allowed to attribute the relevance of each technique with the different proteins. We showed here that the three techniques were reliable for HSA and HRP while only one technique was relevant for IgG and PLL, respectively the BCA and FITC labelling. Regarding physicochemical properties and chemical process aspects, after setting up the working FWR (71% for HSA, 85% for HRP and IgG and 142% for PLL) DLS and zeta potential experiments indicated a good colloidal stability of the STMS@IBAM@Protein.

Preliminary to the sustained protein release study, chemical engineering aspects of the synthesis of STMS@IBAM@Protein NPs, such as scale-up, reproducibility and stability over washings, were investigated with standardized protocols. Then, we showed that such STMS@IBAM@Protein were very efficient and promising materials for sustained protein release (HSA and HRP) upon incubation in HEPES buffer during four days at three different temperatures (25, 37 and 45 °C). The release conditions achieved in *closed (static)* and *opened (dynamic) systems* mimicking respectively equilibrium and continuous flow presented both a burst release after the first 24 h, but the continuous protein release was demonstrated in the dynamic conditions while immobilized protein did not release further in the static conditions.

Furthermore, the enzymatic activity of HRP either immobilized on

the NPs or released was assessed and showed that the protein can still preserve and ensure its biological function for potential therapeutic application.

Finally, an AFM-force spectroscopy study was used as a relevant technique allowing to quantify the weak interactions at play in the adsorption of HSA and HRP on the NPs at the nanoscale. The IBAM-protein interactions were investigated by functionalizing the AFM tip with HSA and HRP proteins. The results suggested different modes of interactions involved between proteins and STMS@IBAM NPs. HSA would interact merely from a combination of several non-covalent forces (electrostatic, hydrogen bonding and hydrophobic interactions) while HRP would interact merely through hydrogen bonding. These results could explain the different adsorption levels of these proteins on STMS@IBAM NPs as well as the higher burst release observed for HSA compared to HRP.

In the future, the combination of magnetic NPs with such IBAM-functionalized STMS as core-shell NPs could lead to a bi-functional therapeutic system ensuring MRI, hyperthermia and protein sustained release for anticancer applications. Indeed, as no influence of the temperature could be seen on the release of proteins, the use of magnetic hyperthermia with an IO@STMS@IBAM@Protein NPs could be performed without impacting the release of therapeutic proteins.

CRediT authorship contribution statement

Joëlle Bizeau: Conceptualization, Data curation, Formal analysis, Investigation, Methodology, Visualization, Writing – original draft, Writing – review & editing. **Alexandre Adam:** Formal analysis, Methodology. **Clémence Nadal:** Data curation, Formal analysis, Investigation, Methodology. **Grégory Francius:** Methodology, Supervision, Validation, Writing – original draft. **David Siniscalco:** Data curation, Formal analysis, Methodology. **Matthias Pauly:** Methodology, Resources, Writing – review & editing. **Sylvie Bégin-Colin:** Resources, Writing – review & editing. **Damien Mertz:** Conceptualization, Funding acquisition, Investigation, Methodology, Resources, Supervision, Validation, Writing – original draft, Writing – review & editing.

Declaration of Competing Interest

The authors declare that they have no known competing financial interests or personal relationships that could have appeared to influence the work reported in this paper.

Data availability

Data will be made available on request.

Acknowledgements

D.M. acknowledges the Materials Institute Carnot Alsace (project ProtRemote) and the Agence Nationale de la Recherche (grant ANR-19-09CE-0004—Corelmag) for financial supports. The spectroscopy and the transmission electronic microscopy platforms of the IPCMS are acknowledged for technical supports.

Appendix A. Supplementary data

Supplementary data to this article can be found online at https://doi.org/10.1016/j.ijpx.2022.100130.

References

Adam, A., Parkhomenko, K., Duenas-Ramirez, P., Nadal, C., Cotin, G., Zorn, P.-E., Choquet, P., Bégin-Colin, S., Mertz, D., 2021. Orienting the pore morphology of core-shell magnetic mesoporous silica with the sol-gel temperature. Influence on MRI and magnetic hyperthermia properties. Molecules 26, 971. https://doi.org/10.3390/molecules26040971.

Alexis, F., Pridgen, E., Molnar, L.K., Farokhzad, O.C., 2008. Factors affecting the clearance and biodistribution of polymeric nanoparticles. Mol. Pharm. 5, 505–515. https://doi.org/10.1021/mp800051m.

Argyo, C., Weiss, V., Bräuchle, C., Bein, T., 2014. Multifunctional mesoporous silica nanoparticles as a universal platform for drug delivery. Chem. Mater. 26, 435–451. https://doi.org/10.1021/cm402592t.

Berglund, G.I., Carlsson, G.H., Smith, A.T., Szöke, H., Henriksen, A., Hajdu, J., 2002. The catalytic pathway of horseradish peroxidase at high resolution. Nature 417, 463–468. https://doi.org/10.1038/417463a.

Bizeau, J., Mertz, D., 2021. Design and applications of protein delivery systems in nanomedicine and tissue engineering. Adv. Colloid Interf. Sci. 287, 102334 https://doi.org/10.1016/j.cis.2020.102334.

Bizeau, J., Adam, A., Bégin, S., Mertz, D., 2021. Serum albumin antifouling effects of Hydroxypropyl-cellulose and Pluronic F127 adsorbed on isobutyramide-grafted stellate silica nanoparticles. Eur. J. Inorg. Chem. https://doi.org/10.1002/ejic.202100678 ejic.202100678.

Cappella, B., Dietler, G., 1999. Force-distance curves by atomic force microscopy. Surf. Sci. Rep. 34, 1–104. https://doi.org/10.1016/S0167-5729(99)00003-5.

Carter, D.C., Ho, J.X., 1994. Structure of serum albumin. In: Advances in Protein Chemistry. Elsevier, pp. 153–203. https://doi.org/10.1016/S0065-3233(08)60640-3.

Chaplin, H., Cohen, S., Press, E., 1965. Preparation and properties of the peptide chains of normal human 19 s γ-globulin (IGM). Biochem. J. 95, 256–261. https://doi.org/10.1042/bj0950256.

Chen, Y., Barkley, M.D., 1998. Toward understanding tryptophan fluorescence in proteins. Biochemistry 37, 9976–9982. https://doi.org/10.1021/bi980274n.

Chen, G., Teng, Z., Su, X., Liu, Y., Lu, G., 2015. Unique biological degradation behavior of stöber mesoporous silica nanoparticles from their interiors to their exteriors. J. Biomed. Nanotechnol. 11, 722–729. https://doi.org/10.1166/jbn.2015.2072.

Chen, W., Tian, R., Xu, C., Yung, B.C., Wang, G., Liu, Y., Ni, Q., Zhang, F., Zhou, Z., Wang, J., Niu, G., Ma, Y., Fu, L., Chen, X., 2017. Microneedle-array patches loaded with dual mineralized protein/peptide particles for type 2 diabetes therapy. Nat. Commun. 8, 1–11. https://doi.org/10.1038/s41467-017-01764-1.

Cotin, G., Kiefer, C., Perton, F., Ihiawakrim, D., Blanco-Andujar, C., Moldovan, S., Lefevre, C., Ersen, O., Pichon, B., Mertz, D., Bégin-Colin, S., 2018. Unravelling the thermal decomposition parameters for the synthesis of anisotropic iron oxide nanoparticles. Nanomaterials 8, 881. https://doi.org/10.3390/nano8110881.

Croissant, J.G., Fatieiev, Y., Khashab, N.M., 2017. Degradability and clearance of silicon, organosilica, silsesquioxane, silica mixed oxide, and mesoporous silica nanoparticles. Adv. Mater. 29, 1604634. https://doi.org/10.1002/adma.201604634.

De Mey, M., Lequeux, G.J., Maertens, J., De Muynck, C.I., Soetaert, W.K., Vandamme, E. J., 2008. Comparison of protein quantification and extraction methods suitable for *E. coli* cultures. Biologicals 36, 198–202. https://doi.org/10.1016/j.biologicals.2007.10.001.

Duenas-Ramirez, P., Bertagnolli, C., Müller, R., Sartori, K., Boos, A., Elhabiri, M., Bégin-Colin, S., Mertz, D., 2020. Highly chelating stellate mesoporous silica nanoparticles for specific iron removal from biological media. J. Colloid Interface Sci. 579, 140–151. https://doi.org/10.1016/j.jcis.2020.06.013.

Francius, G., Alsteens, D., Dupres, V., Lebeer, S., De Keersmaecker, S., Vanderleyden, J., Gruber, H.J., Dufrêne, Y.F., 2009. Stretching polysaccharides on live cells using single molecule force spectroscopy. Nat. Protoc. 4, 939–946. https://doi.org/10.1038/nprot.2009.65.

Gajhede, M., Schuller, D.J., Henriksen, A., Smith, A.T., Poulos, T.L., 1997. Crystal structure of horseradish peroxidase C at 2.15 Å resolution. Nat. Struct. Mol. Biol. 4, 1032–1038. https://doi.org/10.1038/nsb1297-1032.

Greenfield, N.J., Fasman, G.D., 1969. Computed circular dichroism spectra for the evaluation of protein conformation. Biochemistry 8, 4108–4116. https://doi.org/10.1021/bi00838a031.

Hao, N., Liu, H., Li, Linlin, Chen, D., Li, Laifeng, Tang, F., 2012. *In Vitro* degradation behavior of silica nanoparticles under physiological conditions. J Nanosci Nanotechnol 12, 6346–6354. https://doi.org/10.1166/jnn.2012.6199.

He, X.M., Carter, D.C., 1992. Atomic structure and chemistry of human serum albumin. Nature 358, 209–215. https://doi.org/10.1038/358209a0.

Higuchi, A., Aoki, N., Yamamoto, T., Miyazaki, T., Fukushima, H., Tak, T.M., Jyujyoji, S., Egashira, S., Matsuoka, Y., Natori, S.H., 2006. Temperature-induced cell detachment on immobilized pluronic surface. J. Biomed. Mater. Res. 79A, 380–392. https://doi.org/10.1002/jbm.a.30773.

Hinterdorfer, P., Dufrêne, Y.F., 2006. Detection and localization of single molecular recognition events using atomic force microscopy. Nat. Methods 3, 347–355. https://doi.org/10.1038/nmeth871.

Hsiao, L.-W., Lai, Y.-D., Lai, J.-T., Hsu, C.-C., Wang, N.-Y., Wang, S.S., Jan, J.-S., 2017. Cross-linked polypeptide-based gel particles by emulsion for efficient protein encapsulation. Polymer 115, 261–272. https://doi.org/10.1016/j.polymer.2017.03.055.

Huang, A., Wei, B., Mo, J., Wang, Y., Ma, L., 2018. Conformation and activity alteration of horseradish peroxidase induced by the interaction with gene carrier polyethyleneimines. Spectrochim. Acta A Mol. Biomol. Spectrosc. 188, 90–98. https://doi.org/10.1016/j.saa.2017.06.046.

Janshoff, A., Neitzert, M., Oberdörfer, Y., Fuchs, H., 2000. Force spectroscopy of molecular systems—single molecule spectroscopy of polymers and biomolecules. Angew. Chem. Int. Ed. 39, 3212–3237. https://doi.org/10.1002/1521-3773(20000915)39:18<3212::AID-ANIE3212>3.0.CO;2-X.

Klugerman, M.R., 1965. Chemical and physical variables affecting the properties of fluorescein isothiocyanate and its protein conjugates. J. Immunol. 95, 1165–1173.

Knight, M.I., Chambers, P.J., 2003. Problems associated with determining protein concentration: a comparison of techniques for protein estimations. MB 23, 19–28. https://doi.org/10.1385/MB:23:1:19.
Kobsa, S., Saltzman, W.M., 2008. Bioengineering approaches to controlled protein delivery. Pediatr. Res. 63, 513–519. https://doi.org/10.1203/PDR.0b013e318165f14d.
Kumari, M., Maurya, J.K., Tasleem, M., Singh, P., Patel, R., 2014. Probing HSA-ionic liquid interactions by spectroscopic and molecular docking methods. J. Photochem. Photobiol. B Biol. 138, 27–35. https://doi.org/10.1016/j.jphotobiol.2014.05.009.
Leader, B., Baca, Q.J., Golan, D.E., 2008. Protein therapeutics: a summary and pharmacological classification. Nat. Rev. Drug Discov. 7, 21–39. https://doi.org/10.1038/nrd2399.
Maciążek-Jurczyk, M., Szkudlarek, A., Chudzik, M., Pożycka, J., Sułkowska, A., 2018. Alteration of human serum albumin binding properties induced by modifications: a review. Spectrochim. Acta A Mol. Biomol. Spectrosc. 188, 675–683. https://doi.org/10.1016/j.saa.2017.05.023.
Manzano, M., Vallet-Regí, M., 2020. Mesoporous silica nanoparticles for drug delivery. Adv. Funct. Mater. 30, 1902634. https://doi.org/10.1002/adfm.201902634.
McAvan, B.S., Khuphe, M., Thornton, P.D., 2017. Polymer hydrogels for glutathione-mediated protein release. Eur. Polym. J. 87, 468–477. https://doi.org/10.1016/j.eurpolymj.2016.09.032.
Meloun, B., Morávek, L., Kostka, V., 1975. Complete amino acid sequence of human serum albumin. FEBS Lett. 58, 134–137. https://doi.org/10.1016/0014-5793(75)80242-0.
Mertz, D., Tan, P., Wang, Y., Goh, T.K., Blencowe, A., Caruso, F., 2011. Bromoisobutyramide as an intermolecular surface binder for the preparation of free-standing biopolymer assemblies. Adv. Mater. 23, 5668–5673. https://doi.org/10.1002/adma.201102890.
Mertz, D., Cui, J., Yan, Y., Devlin, G., Chaubaroux, C., Dochter, A., Alles, R., Lavalle, P., Voegel, J.C., Blencowe, A., Auffinger, P., Caruso, F., 2012a. Protein capsules assembled via isobutyramide grafts: sequential growth, biofunctionalization, and cellular uptake. ACS Nano 6, 7584–7594. https://doi.org/10.1021/nn302024t.
Mertz, D., Wu, H., Wong, J.S., Cui, J., Tan, P., Alles, R., Caruso, F., 2012b. Ultrathin, bioresponsive and drug-functionalized protein capsules. J. Mater. Chem. 22, 21434–21442. https://doi.org/10.1039/C2JM33737A.
Mertz, D., Affolter-Zbaraszczuk, C., Barthès, J., Cui, J., Caruso, F., Baumert, T.F., Voegel, J.-C., Ogier, J., Meyer, F., 2014. Templated assembly of albumin-based nanoparticles for simultaneous gene silencing and magnetic resonance imaging. Nanoscale 6, 11676–11680. https://doi.org/10.1039/C4NR02623C.
Micsonai, A., Wien, F., Kernya, L., Lee, Y.-H., Goto, Y., Réfrégiers, M., Kardos, J., 2015. Accurate secondary structure prediction and fold recognition for circular dichroism spectroscopy. Proc. Natl. Acad. Sci. U. S. A. 112, E3095–E3103. https://doi.org/10.1073/pnas.1500851112.
Micsonai, A., Wien, F., Bulyáki, É., Kun, J., Moussong, É., Lee, Y.-H., Goto, Y., Réfrégiers, M., Kardos, J., 2018. BeStSel: a web server for accurate protein secondary structure prediction and fold recognition from the circular dichroism spectra. Nucleic Acids Res. 46, W315–W322. https://doi.org/10.1093/nar/gky497.
Micsonai, A., Bulyáki, É., Kardos, J., 2021. BeStSel: from secondary structure analysis to protein fold prediction by circular dichroism spectroscopy. In: Chen, Y.W., Yiu, C.-P. B. (Eds.), Structural Genomics. Springer US, New York, NY, pp. 175–189. https://doi.org/10.1007/978-1-0716-0892-0_11.
Möller, K., Bein, T., 2019. Degradable drug carriers: vanishing mesoporous silica nanoparticles. Chem. Mater. 31, 4364–4378. https://doi.org/10.1021/acs.chemmater.9b00221.
Mumcuoglu, D., de Miguel, L., Jekhmane, S., Siverino, C., Nickel, J., Mueller, T.D., van Leeuwen, J.P., van Osch, G.J., Kluijtmans, S.G., 2018. Collagen I derived recombinant protein microspheres as novel delivery vehicles for bone morphogenetic protein-2. Mater. Sci. Eng. C 84, 271–280. https://doi.org/10.1016/j.msec.2017.11.031.
Noble, J.E., Bailey, M.J.A., 2009. Chapter 8 quantitation of protein. In: Methods in Enzymology. Elsevier, pp. 73–95. https://doi.org/10.1016/S0076-6879(09)63008-1.
Olson, B.J.S.C., Markwell, J., 2007. Assays for determination of protein concentration. Current Protocols in Protein Science 48. https://doi.org/10.1002/0471140864.ps0304s48.
Omar, H., Croissant, J.G., Alamoudi, K., Alsaiari, S., Alradwan, I., Majrashi, M.A., Anjum, D.H., Martins, P., Laamarti, R., Eppinger, J., Moosa, B., Almalik, A., Khashab, N.M., 2017. Biodegradable magnetic Silica@Iron oxide nanovectors with ultra-large mesopores for high protein loading, magnetothermal release, and delivery. In: Journal of Controlled Release, 4th Symposium on Innovative Polymers for Controlled Delivery (SIPCD 2016), 23–26 September 2016, Suzhou, China, 259, pp. 187–194. https://doi.org/10.1016/j.jconrel.2016.11.032.
Papadea, C., Check, I.J., 1989. Human immunoglobulin G and immunoglobulin G subclasses: biochemical, genetic, and clinical aspects. Crit. Rev. Clin. Lab. Sci. 27, 27–58. https://doi.org/10.3109/10408368909106589.
Perton, F., Harlepp, S., Follain, G., Parkhomenko, K., Goetz, J.G., Bégin-Colin, S., Mertz, D., 2019a. Wrapped stellate silica nanocomposites as biocompatible luminescent nanoplatforms assessed in vivo. J. Colloid Interface Sci. 542, 469–482. https://doi.org/10.1016/j.jcis.2019.01.098.
Perton, F., Tasso, M., Muñoz Medina, G.A., Ménard, M., Blanco-Andujar, C., Portiansky, E., van Raap, M.B.F., Bégin, D., Meyer, F., Begin-Colin, S., Mertz, D., 2019b. Fluorescent and magnetic stellate mesoporous silica for bimodal imaging and magnetic hyperthermia. Appl. Mater. Today 16, 301–314. https://doi.org/10.1016/j.apmt.2019.06.006.
Putney, S.D., Burke, P.A., 1998. Improving protein therapeutics with sustained-release formulations. Nat. Biotechnol. 16, 153–157. https://doi.org/10.1038/nbt0298-153.
Saphire, E.O., Parren, P.W.H.I., Pantophlet, R., Zwick, M.B., Morris, G.M., Rudd, P.M., Dwek, R.A., Stanfield, R.L., Burton, D.R., Wilson, I.A., 2001. Crystal structure of a neutralizing human IgG against HIV-1: a template for vaccine design. Science. https://doi.org/10.1126/science.1061692.
Schejter, A., Lanir, A., Epstein, N., 1976. Binding of hydrogen donors to horseradish peroxidase: a spectroscopic study. Arch. Biochem. Biophys. 174, 36–44. https://doi.org/10.1016/0003-9861(76)90321-0.
Shahabadi, N., Khorshidi, A., Moghadam, N.H., 2013. Study on the interaction of the epilepsy drug, zonisamide with human serum albumin (HSA) by spectroscopic and molecular docking techniques. Spectrochim. Acta A Mol. Biomol. Spectrosc. 114, 627–632. https://doi.org/10.1016/j.saa.2013.05.092.
Shitole, A.A., Raut, P., Giram, P., Rade, P., Khandwekar, A., Garnaik, B., Sharma, N., 2020. Poly (vinylpyrrolidone)-iodine engineered poly (ε-caprolactone) nanofibers as potential wound dressing materials. Mater. Sci. Eng. C 110, 110731. https://doi.org/10.1016/j.msec.2020.110731.
Smith, P.K., Krohn, R.I., Hermanson, G.T., Mallia, A.K., Gartner, F.H., Provenzano, M.D., Fujimoto, E.K., Goeke, N.M., Olson, B.J., Klenk, D.C., 1985. Measurement of protein using bicinchoninic acid. Anal. Biochem. 150, 76–85. https://doi.org/10.1016/0003-2697(85)90442-7.
Stoscheck, C.M., 1990. [6] Quantitation of protein. In: Methods in Enzymology. Elsevier, pp. 50–68. https://doi.org/10.1016/0076-6879(90)82008-P.
Sudlow, G., Birkett, D.J., Wade, D.N., 1975. The characterization of two specific drug binding sites on human serum albumin. Mol. Pharmacol. 11, 824–832.
Sugio, S., Kashima, A., Mochizuki, S., Noda, M., Kobayashi, K., 1999. Crystal structure of human serum albumin at 2.5 Å resolution. Protein Eng. Des. Sel. 12, 439–446. https://doi.org/10.1093/protein/12.6.439.
Tang, F., Li, L., Chen, D., 2012. Mesoporous silica nanoparticles: synthesis, biocompatibility and drug delivery. Adv. Mater. 24, 1504–1534. https://doi.org/10.1002/adma.201104763.
Tong, Z., Zhou, J., Zhong, J., Tang, Q., Lei, Z., Luo, H., Ma, P., Liu, X., 2018. Glucose- and H2O2-Responsive polymeric vesicles integrated with microneedle patches for glucose-sensitive transcutaneous delivery of Insulin in diabetic rats. ACS Appl. Mater. Interfaces 10, 20014–20024. https://doi.org/10.1021/acsami.8b04484.
Trynda-Lemiesz, L., 2004. Paclitaxel–HSA interaction. Binding sites on HSA molecule. Bioorg. Med. Chem. 12, 3269–3275. https://doi.org/10.1016/j.bmc.2004.03.073.
Tuncaboylu, D.C., Friess, F., Wischke, C., Lendlein, A., 2018. A multifunctional multimaterial system for on-demand protein release. J. Control. Release 284, 240–247. https://doi.org/10.1016/j.jconrel.2018.06.022.
Vander Straeten, A., Dupont-Gillain, C., 2020. Self-reorganizing multilayer to release free proteins from self-assemblies. Langmuir 36, 972–978. https://doi.org/10.1021/acs.langmuir.9b03547.
Veitch, N.C., 2004. Horseradish peroxidase: a modern view of a classic enzyme. Phytochemistry 65, 249–259. https://doi.org/10.1016/j.phytochem.2003.10.022.
Vivian, J.T., Callis, P.R., 2001. Mechanisms of tryptophan fluorescence shifts in proteins. Biophys. J. 80, 2093–2109. https://doi.org/10.1016/S0006-3495(01)76183-8.
Walker, J.M., 2009. The bicinchoninic acid (BCA) assay for protein quantitation. In: Walker, J.M. (Ed.), The Protein Protocols Handbook, Springer Protocols Handbooks. Humana Press, Totowa, NJ, pp. 11–15. https://doi.org/10.1007/978-1-59745-198-7_3.
Wang, R., Yang, Z., Luo, J., Hsing, I.-M., Sun, F., 2017. B12-dependent photoresponsive protein hydrogels for controlled stem cell/protein release. PNAS 114, 5912–5917. https://doi.org/10.1073/pnas.1621350114.
Wang, J., Tian, L., Chen, N., Ramakrishna, S., Mo, X., 2018. The cellular response of nerve cells on poly-l-lysine coated PLGA-MWCNTs aligned nanofibers under electrical stimulation. Mater. Sci. Eng. C 91, 715–726. https://doi.org/10.1016/j.msec.2018.06.025.
Welinder, K.G., 1976. Covalent structure of the glycoprotein horseradish peroxidase (EC 1.11.1.7). FEBS Lett. 72, 19–23. https://doi.org/10.1016/0014-5793(76)80804-6.
Wiberg, K., Sterner-Molin, A., Jacobsson, S.P., 2004. Simultaneous determination of albumin and immunoglobulin G with fluorescence spectroscopy and multivariate calibration. Talanta 62, 567–574. https://doi.org/10.1016/j.talanta.2003.08.024.
Wu, S.-H., Mou, C.-Y., Lin, H.-P., 2013. Synthesis of mesoporous silica nanoparticles. Chem. Soc. Rev. 42, 3862–3875. https://doi.org/10.1039/c3cs35405a.
Wu, J., Chen, Yan, Wang, Y., Yin, H., Zhao, Z., Liu, N., Xie, M., Chen, Yiping, 2017a. Poly-L-lysine brushes on magnetic nanoparticles for ultrasensitive detection of *Escherichia coli* O157: H7. Talanta 172, 53–60. https://doi.org/10.1016/j.talanta.2017.05.035.
Wu, D.-Y., Ma, Y., Hou, X.-S., Zhang, W.-J., Wang, P., Chen, H., Li, B., Zhang, C., Ding, Y., 2017b. Co-delivery of antineoplastic and protein drugs by chitosan nanocapsules for a collaborative tumor treatment. Carbohydr. Polym. 157, 1470–1478. https://doi.org/10.1016/j.carbpol.2016.11.027.
Xu, C., Wei, Z., Gao, H., Bai, Y., Liu, H., Yang, H., Lai, Y., Yang, L., 2017. Bioinspired mechano-sensitive macroporous ceramic sponge for logical drug and cell delivery. Advanced Science 4, 1600410. https://doi.org/10.1002/advs.201600410.
Yu, M., Wu, J., Shi, J., Farokhzad, O.C., 2016. Nanotechnology for protein delivery: overview and perspectives. Journal of Controlled Release, SI: North America Part II 240, 24–37. https://doi.org/10.1016/j.jconrel.2015.10.012.
Zaguri, M., Kandel, S., Rinehart, S.A., Torsekar, V.R., Hawlena, D., 2021. Protein quantification in ecological studies: a literature review and empirical comparisons of standard methodologies. Methods Ecol. Evol. 12, 1240–1251. https://doi.org/10.1111/2041-210X.13601.
Zhang, Y., Zhang, J., Huang, X., Zhou, X., Wu, H., Guo, S., 2012. Assembly of graphene oxide–enzyme conjugates through hydrophobic interaction. Small 8, 154–159. https://doi.org/10.1002/smll.201101695.
Zhang, K., Xu, L.-L., Jiang, J.-G., Calin, N., Lam, K.-F., Zhang, S.-J., Wu, H.-H., Wu, G.-D., Albela, B., Bonneviot, L., Wu, P., 2013a. Facile large-scale synthesis of monodisperse

mesoporous silica nanospheres with tunable pore structure. J. Am. Chem. Soc. 135, 2427–2430. https://doi.org/10.1021/ja3116873.

Zhang, D., Zhang, Y., Zheng, L., Zhan, Y., He, L., 2013b. Graphene oxide/poly-l-lysine assembled layer for adhesion and electrochemical impedance detection of leukemia K562 cancercells. Biosens. Bioelectron. 42, 112–118. https://doi.org/10.1016/j.bios.2012.10.057.

Zhang, Y., Chi, C., Huang, X., Zou, Q., Li, X., Chen, L., 2017. Starch-based nanocapsules fabricated through layer-by-layer assembly for oral delivery of protein to lower gastrointestinal tract. Carbohydr. Polym. 171, 242–251. https://doi.org/10.1016/j.carbpol.2017.04.090.

Zhang, Yi, Tong, C., Ma, Z., Lu, L., Fu, H., Pan, S., Tong, W., Li, X., Zhang, Yihe, An, Q., 2019. A self-powered delivery substrate boosts active enzyme delivery in response to human movements. Nanoscale 11, 14372–14382. https://doi.org/10.1039/C9NR04673A.

Zheng, S., Guan, Y., Yu, H., Huang, G., Zheng, C., 2019. Poly-ʟ-lysine-coated PLGA/poly (amino acid)-modified hydroxyapatite porous scaffolds as efficient tissue engineering scaffolds for cell adhesion, proliferation, and differentiation. New J. Chem. 43, 9989–10002. https://doi.org/10.1039/C9NJ01675A.